Spring 5-2018

Investigating Mechanisms of Hydraulic Conductivity Transience in Sandy Streambeds

Wilhelm Fraundorfer
University of Nebraska - Lincoln, wfraundorfer@huskers.unl.edu

INVESTIGATING MECHANISMS OF HYDRAULIC CONDUCTIVITY TRANSIENCE IN SANDY STREAMBEDS

by

Wilhelm P. Fraundorfer

A Thesis

Presented to the Faculty of

The Graduate College at the University of Nebraska

In Partial Fulfillment of Requirements

For the Degree of Master of Science

Major: Natural Resource Sciences

Under the Supervision of Professor Jesse T. Korus

Lincoln, Nebraska

May, 2018

INVESTIGATING MECHANISMS OF HYDRUALIC CONDUCTIVITY TRANSIENCE IN SANDY STREAMBEDS

Wilhelm P. Fraundorfer, M.S.

University of Nebraska, 2018

Advisor: Jesse T. Korus

Streambed hydraulic conductivity (*K*) is known to be spatially and temporally heterogeneous, but few attempts to understand the controls on temporal variability have been made. This study documents temporal *K* transience and demonstrates how hydraulic, geophysical, and sedimentological methods can be combined to understand the processes that give rise to changes in streambed *K*. Falling head permeameter tests and slug tests were conducted to determine vertical *K* (K_v) and *K* (slug test *K*), respectively. These tests were repeated three times over a twelve-week period on the same grid at a depth of 0.5 meters below the bed of the Loup River in east-central Nebraska during the summer of 2017. This grid included (1) a stationary braid bar where diagenetic pore clogging is expected to control *K* transience, and (2) mobile sediments of the adjacent stream channel where deposition and erosion are thought to be the dominant controls. Sediment samples were collected at the site of each hydraulic test to determine grain size distributions and estimate *K*. Ground penetrating radar surveys at 450 MHz and frequency domain electromagnetic geophysical surveys provided high resolution images of subsurface structure. K_v ranges between 0.1 and 45 meters/day, and *K* ranges between 15 and 55 meters/day. K_v and *K* changed significantly only between the second and third sampling events. *K* declined 14-20% in both environments while K_v declined 27% on the

bar, but was unchanged in the channel. Despite evidence of scour and fill in the channel captured by GPR, deposition and erosion did not exert a dominant influence on *K* transience. The results of this study suggest that processes other than physical sediment transport, such as bioclogging or gas ebullition, were responsible for the decrease in *K*.

AUTHOR'S ACKNOWLEDGEMENTS

I would like to recognize several people who helped see this thesis to completion. First, my adviser, Jesse Korus, has provided guidance and wisdom throughout the entire process of developing and writing this thesis. It is fair to say that this research could not have even been conceived of without him. Vitaly Zlotnik and Troy Gilmore provided invaluable advice and technical assistance in the classroom, in the laboratory, and in the field. I would also like to acknowledge the contribution of Kelsey Karnik, who's assistance with statistical analyses added significant quality to this thesis. Heidi Hensen is completely responsible for my decision to pursue a graduate degree at all. Heidi also provided invaluable motivation and support throughout my work on this research.

I would also like to recognize the outstanding efforts of Robert Clarke and Alexa Davis. These two were hired on to help with the field work and data processing during the summer and fall of 2017. This project absolutely could not have been completed without these two fantastic individuals. Throughout the summer I came to rely on the conscientiousness, intelligence, and positive attitude of these people who I now call my friends. I cannot thank the two of them enough for putting up with me and this crazy project all summer.

GRANT INFORMATION

This research was supported by the following grants in 2017:

1. **GSA Graduate Student Research Grant** – Awarded by the Geological Society of America to support graduate student theses and dissertations that focus on geological research.

2. **The GSSI Student Research Grant** – Awarded by the Near Surface Geophysics focus group of the American Geophysical Union, through the generosity of GSSI, in support of student research that utilizes near surface geophysical methods.

3. **The Yatkola-Edwards Grant** – Awarded by the Nebraska Geological Society in support of graduate and undergraduate geological research.

This research may not have been possible, and certainly not would have been as successful or comprehensive as it is without the aid of the grants listed above. My adviser and I would like to extended our gratitude to the organizations above who deemed our research worthy of financial support. These are examples of generosity and solidarity that are extremely important within geology and academia in general.

TABLE OF CONTENTS

LIST OF VARIABLES

b – Aquifer saturated thickness.
C_s – Streambed conductance (MODFLOW)
c – Empirical coefficient in the Hazen equation for hydraulic conductivity.
D – Diameter of permeameter.
d – Depth of streambed in MODFLOW cell.
d_{10} – Diameter at which 10% of the particles in a sediment sample are finer.
d_{50} – Diameter at which 50% of the particles in a sediment sample are finer.
H_0 – Displacement at time 0.
H_1 – Displacement at time 1.
K – Hydraulic conductivity from Bouwer & Rice slug test and empirical calculations.
K_h – Horizontal hydraulic conductivity.
$K_{streambed}$ – Hydraulic conductivity of streambed in MODFLOW.
K_v – Vertical hydraulic conductivity from falling head permeameter test.
k – Intrinsic permeability
L – Length of sediment being tested by permeameter.
L^* - Length of the screened interval of a well.
l – Length of streambed in MODFLOW cell.
m – Aquifer anisotropy given by: $\sqrt{K_h / K_v}$
Q – Volume per time inflow of water into a well.
t_0 – Time at which permeameter test begins.
t_1 – Time at which first head measurement is made.
t – Time over which water level recovery is recorded in a well.
r_c – Interior radius of well.
R_e – Effective well radius.
r_w – Radius of well casing.
w – Width of streambed in MODFLOW cell.
y – Distance between water level in a well and the equilibrium water table level.
y_0 – Unit length drop in water level in a well at time zero after slug displacement.
y_t – Unit length drop in water level in a well at time t after slug displacement.

LIST OF MULTIMEDIA OBJECTS

CHAPTER 1.0 INTRODUCTION AND REVIEW OF LITERATURE

Characterization of the heterogeneity in aquifer hydraulic conductivity (*K*) has become a fundamental pursuit of hydrogeology. Increasingly, *K* characterization involves collaboration between hydrogeologists, sedimentologists, and geophysicists (Koltermann and Gorelick 1996; Huggenberger and Aigner 1999; de Marsily et al. 2005; Eaton 2006). Streams represent an important constant head boundary condition in many groundwater models, and as such their *K* heterogeneity has direct implications on hydrogeological models. The streambed is an inherently dynamic environment that needs to be characterized both spatially and temporally to accurately understand the active processes responsible for streambed *K* heterogeneity.

1.1 Characterizing *K* Heterogeneity

Heterogeneity can be defined as the *K* of an aquifer being spatially variable, or the opposite of *K* homogeneity. *K* heterogeneity plays a significant role in determining how groundwater flows in aquifers (Eaton 2006). High *K* zones act as preferential flow paths that complicate the prediction of groundwater movement and contaminant transport. Heterogeneity of *K* gives rise to a parameter used extensively in contaminant hydrogeology known as dispersivity, which describes the tendency of dissolved solutes in groundwater to creep ahead or lag behind of the main advective front of a plume (Domenico and Schwartz 1990). There are numerous parallels between work that has been done in the petroleum industry for decades, and what needs to be done to improve *K* characterization in hydrogeology (Koltermann and Gorelick 1996; Huggenberger and Aigner 1999; de Marsily et al. 2005; Eaton 2006). As technology improves and the cost

of characterization drops, the methods being employed by the petroleum industry are becoming available to hydrogeologists.

Aquifer heterogeneity has been modeled primarily using three methods: structure imitating, process imitating, and descriptive methods (Koltermann and Gorelick 1996). Structure imitating methods rely on matching geostatistical results to known sedimentary geometries (Koltermann and Gorelick 1996). Process imitating methods utilize aquifer model calibration and geologic process models (Koltermann and Gorelick 1996). Process imitating methods attempt to calibrate flow models with measured aquifer hydraulic properties or combine the laws of physics with sedimentology to predict particle size distributions in deposits. Descriptive methods separate an aquifer into zones of similar hydraulic properties based on field observations (Koltermann and Gorelick 1996).

1.2 Importance of Streambed *K* Heterogeneity

Streambeds play an important role in both hydrology and ecology by controlling groundwater-surface water interactions. The streambed is the interface between active stream channels and the underlying alluvial aquifer, and as a result, its hydrologic properties play a significant role in regulating the exchange of water and solutes between the two domains. The characteristics of streambeds have a considerable influence on the stream drawdown from pumping wells in alluvial aquifers (Zlotnik et al. 1999). Streambed hydraulic properties also play a role in determining the efficiency of bank filtration processes (Heberer et al. 2011). The hydraulic properties of streambeds are generalized in MODFLOW by the streambed conductance (C_s) value. (Pérez-Paricio et al. 2010). Streambed conductance is given by:

$$(1)\ C_s = K_{streambed}\frac{wl}{d}$$

Where w is streambed width, l is streambed length, and d is streambed depth. In MODFLOW, C_s values are assumed to be homogenous in both space and time, which is known to be unrealistic (Genereux et al. 2008). For regional groundwater models the realistic variability of C_s may be of little importance, but for smaller scale models that quantify groundwater and surface-water interactions, the assumption could be significant for understanding localized or seasonal fluxes.

Biologically, the area around a stream where groundwater and surface water are exchanged is known as the hyporheic zone (Boulton et al. 1998). The upwelling of nutrients from the streambed can be an important food source for aquatic ecosystems within the stream (Boulton et al. 1998). Downwelling water can be an important source of dissolved oxygen and nutrients for organisms within the hyporheic zone itself (Boulton et al. 1998). Vertical K (K_v) determines the size of the hyporheic zone as well as the rate of exchange of solutes in the hyporheic zone (Valett et al. 1996; Morrice et al. 1997). K_v exerts an important control on the rate of water exchange between the subsurface and a stream. The rate of exchange controls the residence time of nutrients and solutes in the subsurface, which is why understanding K in the hyporheic zone has been of recent interest (Valett et al. 1996).

1.3 Proposed Mechanisms Responsible for Streambed *K* Heterogeneity

The body of literature on heterogeneity characterization in streambeds is relatively limited, and only in the last 10 years have studies attempted to characterize streambed K in both spatial and temporal domains. This research has shown that

streambed *K* is a spatially heterogeneous and temporally dynamic property (Cardenas and Zlotnik 2003a; Cardenas et al. 2004; Jiang et al. 2015). Although a few select studies have recorded changes in streambed *K* over time, the majority of streambed research has focused on spatial characterization or "snapshots" of the heterogeneity geometry at a moment in time. It is generally accepted that in sandy streambeds emplacement of silt and clay particles are primarily responsible for low *K* zones that constitute much of the observed heterogeneity (Springer et al. 1999; Genereux et al. 2008; Nowinski et al. 2011). Despite this agreement, competing hypotheses have been proposed to explain the emplacement of fine particles in sandy streambeds.

Deposition and erosion of fine-grained sediment (silt, clay) within the streambed has been proposed as the dominant mechanism for the development of heterogeneity in streambeds (Sebok et al. 2015; Jiang et al. 2015; Korus et al. 2017). The primary evidence for this has been that greater heterogeneity in *K* is observed along bends in river channels where stream velocity is most variable. *K* heterogeneity is developed in these areas because progressively smaller particles fall out of suspension as flow velocity decreases (Sebok et al. 2015; Jiang et al. 2015).

Sebok et al. (2015) used falling head permeameters and slug tests to directly measure *K* on a straight reach and a meander reach of a stream in Denmark. The results of this work showed that both *K* and K_v were more variable in the meander section of the stream and that *K* was more variable perpendicular to the stream than parallel to it. This study also documented the temporal variability of *K* with datasets from December 2011 and August 2012. Sediment cores were also collected which showed that the presence of

fine organic layers within the streambed sediments was strongly correlated to low K_v measurements.

Jiang et al. (2015) used falling head permeameters in conjunction with grain size analysis to measure K_v along a stream in China at four different sites exhibiting three geomorphological characteristics: straight channels, anabranching channels, and meandering channels. This work showed that the highest K_v values were recorded on the erosional bank and lower values recorded near the depositional bank of the meander channels. Grain size analysis showed that grain size distributions were considerably different on opposite sides of the channels. Grain size data in combination with the K_v data was interpreted to mean that deposition and erosion played a dominant role in shaping the K_v heterogeneity of the studied streambed.

Genereux et al. (2008) conducted a detailed study of the temporal variability of K_v on the West Bear Creek in North Carolina using falling head permeameters. Falling head permeameter tests were made bimonthly over one year along two generally straight reaches of the channel. It was found that streambed K_v was considerably spatially and temporally variable and it was noted that increases and decreases in K_v were recorded after high flow events. Genereux et al. (2008) suggested that deposition and erosion influenced K_v variability by changing the grain size distribution over time.

Levy et al. (2010) conducted a study to measure the effects that storm events have on the riverbank filtration potential of the Miami River in southwest Ohio. Seepage meters and slug testing were used in concert with bathymetric profiles and scour chains to quantify the erosion and change in K caused by 3 storm events between December 2004 and May 2006. Scours as great as one meter were recorded in response to storm events,

but sensitivity analyses showed that changes in K_v recorded over the same period would not have reduced the site's capacity for riverbank filtration.

Others have argued that a diagenetic pore clogging mechanism is responsible for the emplacement of fine particles (Nowinski et al. 2011; Dong et al. 2012). This diagenetic hypothesis asserts that the vertical movement of groundwater in the streambed causes fine particles to be removed, whereas in point bars the interaction of horizontal flow with the unsaturated zone causes fine particles collect (Dong et al. 2012). This diagenetic mechanism has been proposed as an explanation to why *K* is observably higher in the streambed channel relative to point bars (Sebok et al. 2015). Dong et al. reported that K_v values from the edges of a point bar were on average greater than those from the center of the same point bar.

Nowinsky et al. (2011) conducted a study on an artificial meandering river and streambed on campus at the University of Minnesota. Slug testing was performed during the summers of 2008 and 2009 to determine *K* at 37 different permanently installed piezometers in the artificial streambed. Groundwater modeling with particle tracking based on water table elevation data was also used to show where mobilized fine particles would travel during the study period. Locations with initially high *K* were observed to increase in *K* over time, while locations with initially low *K* were seen to decrease over time. Model simulations suggested that mobilized fine particles would have been transported from high *K* zones toward low *K* zones. From this data it was interpreted that fine sediment particles transported by hyporheic groundwater flow were changing the *K* heterogeneity over time from the original hydraulic properties of the deposits.

Dong et al. (2012) conducted falling head permeameter tests to characterize K_v across point bars and the stream channel of Clear Creek in Nebraska. K_v was higher along the edges of the point bars than locations within the point bar, and bar K_v was generally lower than stream channel K_v. Grain size analyses showed slightly greater amounts of silt and clay particles on the point bars relative to the stream channel. The differences in K_v between channel and point bar environments was interpreted to be the result of a diagenetic sediment transport process whereby fine particles are mobilized by vertical groundwater flow in the streambed. Dong et al. (2012) argue that when fine particles are brought into the stream channel, the actively flowing water removes the particles from the sediments and allows pore volume and K_v to remain unchanged. Fine particles accumulate on the point bars due to the dominance of horizontal groundwater flow in the bar sediments, reducing pore space as well as K_v.

Chen et al. (2007) used a laboratory experiment to demonstrate that colloids suspended in pore fluids can aggregate onto a sediment matrix and reduce permeability. Polyethylene tubes packed with glass beads had a suspension containing zirconia (ZrO_2) colloids flushed through them. The tubes were imaged using x-ray difference micro-tomography (XDMT) to determine porosity and specific surface area, from which permeability was calculated using the Kozeny-Carmen relationship. Imaging before and after flushing the tubes showed that porosity and permeability were significantly reduced by accumulations of fine colloids, and that tortuosity increased. This pore scale laboratory research was interpreted as being analogous and applicable to real hydrogeological situations where groundwater containing fine particles move through porous media, such as a streambed.

The presence of gas within streambed sediments has been observed and put forward as a potential source of *K* heterogeneity (Cuthbert et al. 2010; Dong et al. 2012). The presence of gases beneath the water table of a streambed would represent a decrease in the effective porosity of the streambed sediments, as well as a decrease in permeability and *K* (Cuthbert et al. 2010; Dong et al. 2012). Cuthbert et al. (2010) used piezometers installed into a streambed in the United Kingdom, as well as a bespoke device on the submerged sediment-water interface, to measure the volume of gas released by streambed sediments. With minor disturbance of the streambed, gases could be collected using the bespoke device, and gas was also collected from piezometers down to 0.8 meters below the river bed (Cuthbert et al. 2010). A groundwater model developed to take into account the effects of gas content did show greater discharge of groundwater through the channel sides during low-flow conditions when field data suggested that gas content would be lower (Cuthbert et al. 2010).

Dong et al. (2012) noticed "sand rings" and gas bubbles emanating from them during their studies on a Nebraska stream. Denitrification due to redox conditions in streambeds in agricultural areas has been proposed as a source of carbon dioxide in streambed sediments (Cuthbert et al. 2010; Dong et al. 2012). Nitrate also serves as a source of nitrogen gas in streambeds during low oxygen conditions (Cuthbert et al. 2010; Dong et al. 2012). Dong et al. tied in the presence of vertically moving gas bubbles into the diagenetic pore clogging mechanism by explaining that gases help to lift fine particles into the water column of the stream channel. The vertical groundwater and bubble migration beneath the stream channel would also lead to an increase in the effective porosity of sediments beneath the stream channel (Dong et al. 2012). It was proposed that

on bar structures the horizontal flow of groundwater would lead to bubble accumulation near the surface, which would act to exacerbate the catchment of fine particles and decrease *K* (Dong et al. 2012).

Bioclogging refers to the reduction in effective porosity of aquifer sediments by aggregates of bacterial cells and exopolymeric saccharides (Newcomer et al. 2016). Most studies that address bioclogging have modeled it as a pore-scale phenomenon, but it has been assumed to be a potentially significant process affecting permeability in both the saturated and unsaturated zones. Newcomer et al. (2016) attempted to show the potential effect of bioclogging on infiltration in connected and disconnected streams using a 1D transient HYDRUS model. A simple exponential model of biomass generation was assumed that ignores factors such as decay, sorption, and biological consumption. This was combined with grain size distribution data from the Russian River in California for calculation of saturated and unsaturated *K* in HYDRUS. The 1D model showed that flux and *K* decreased considerably with increased bioclogging per the exponential model.

Compaction resulting from the weight of newly deposited sediment atop already present sand bars has the ability to influence the *K* heterogeneity of streambeds (Springer et al. 1999). This hypothesis posits that bars consisting dominantly of sand have a different temporal response to sediment compaction than deposits that contain finer particles. Sand deposits exhibit an elastic rebound and return to pre-deposition *K*, unlike deposits containing finer particles, which tend to exhibit permanent reduction in *K* due to compaction. Figure 1-1 is an illustration of all the streambed processes discussed in this section, it shows hyporheic pore clogging taking place beneath a compound bar and deposition and erosion occurring in the stream channel.

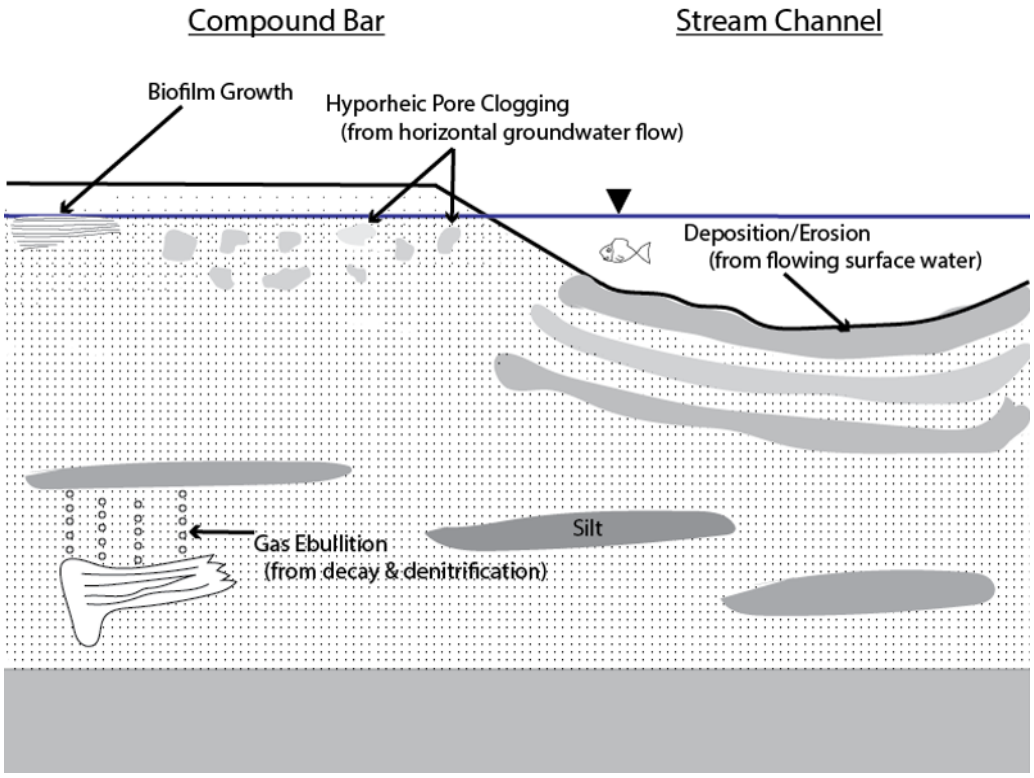

Figure 1-1: Conceptual diagram of streambed processes influencing *K*.

1.4 Methods for Characterizing Streambed *K* Heterogeneity

Studies of streambed *K* heterogeneity have generally focused on direct field measurement of *K* with hydraulic tests at various spatial and temporal scales. The efficacy of slug testing for characterizing streambed *K* heterogeneity has been demonstrated by many authors (Bjerg et al. 1992; Cardenas and Zlotnik 2003a; Conant 2004; Nowinski et al. 2011; Sebok et al. 2015). *K* resulting from slug testing is generally not given a directionality component, although Sebok et al. (2015) did refer to slug test values as horizontal *K* (K_h). Falling head permeameters have been extensively used to characterize the K_v heterogeneity of streambed sediments (Chen 2000; Genereux et al. 2008; Dong et al. 2012; Jiang et al. 2015; Sebok et al. 2015; Korus et al. 2017). Conductivity values resulting from permeameter tests are generally referred to as K_v

because water is forced through the sediment within the open bottom tubes in a primarily vertical direction (Chen 2000).

A constant head injection test was developed that produces more consistent *K* results than slug tests in low permeability streambeds (Cardenas and Zlotnik 2003b). It is important to note that the constant head injection test has demonstrated increasing overestimation of *K* with increasing permeability of the streambed, and constant head is also difficult to maintain when *K* is high (Cardenas and Zlotnik 2003b). It is also possible to utilize potentiomanometers simultaneously with seepage meters to obtain an estimate of streambed *K* (Lee and Cherry 1979).

Choosing which method to characterize streambed *K* requires some knowledge of the general range of *K*, ease of access to the field site, suitability of the streambed, as well as what parameters are of interest. It has been shown that variability between methods is often less than the variability of *K* in streambeds, with the implication being that using a consistent method may be more important than which method is chosen (Landon et al. 2001). Kennedy et al. (2008) published a paper studying the error in interpolations of streambed properties from point measurements that resulted from sampling density and design. Head gradient, K_v, specific discharge, solute concentration, and solute flux point measurements were taken and the average value from interpolation of these parameters was compared with the "true" average from the point measurements. It was found that for stream reach characterization it was necessary to collect between 0.05 and 0.06 points per m^2 to be within 10% of the "true" average from interpolation. Point densities of 0.08 to 0.09 points per m^2 were qualitatively determined to give a realistic image of a

parameter's spatial field, and sampling density was shown to be significantly more important than sampling design in determining error.

1.5 Fluvial Sediment Dynamics

The total amount of solids transported in a fluvial system can be broken into two distinct components: the bed load and suspended load. Bed load refers to the particles that saltate along the bottom of the stream channel; this load is highly flow dependent and difficult to measure (Syvitski et al. 2000). The suspended load refers to particles that are carried within the water column completely supported by flow velocity. Suspended load is highly source dependent and easier to measure. Factors that control the total solid transport of a river include: local vegetation, basin geology, topography, climate, as well as anthropogenic structures.

When a stream is being inundated by a volume of sediment greater than its carrying capacity, the process of aggradation or a "building up" of the surrounding landscape occurs (Leopold and Bull 1979; Dey 2014). When a stream is starved of sediment, erosion is the dominant process and degradation occurs. This is a rather simple characterization of what are actually very complex fluvial processes, factors such as the presence or lack of accommodation space will play a large role in determining whether aggradation or degradation dominate.

Volumes of sediment moving as bed load down a river are typically referred to as "sediment slugs." Sediment slugs are defined as: "Bodies of clastic material associated with disequilibrium conditions in fluvial systems over time periods above the event scale" (Nicholas et al. 1995). Sediment slugs range from the smallest discernable body of

sediment moving down channel, called unit bars (Smith 1974), to large composite bars that are only changed by high magnitude events (Nicholas et al. 1995).

1.6 Experimental Design and Research Hypothesis

Given the sparse research characterizing streambed *K* heterogeneity, and the specific lack of rigorous studies with a temporal focus, there are questions that remain unanswered in this space. One of the primary questions would be; what are the most dominant processes that control the development of streambed *K* heterogeneity over time? The empirical data that has been reported in the body of literature on this topic identifies two competing hypotheses; 1. that deposition and erosion control *K* variability, and 2. that hyporheic pore clogging controls *K* variability. The literature also provides information about which sub-environments of the streambed each process may be the most active: flowing stream channels and meander bends for deposition and erosion, and bar/bank structures for pore clogging (see figure 1-1). From this foundation, an experiment can be conceived that records changes in *K* heterogeneity over time in both environments to determine which is changing at a greater rate, assuming that the identified processes are in fact dominating the change in the given environments. This research attempted to perform such an experiment with the hypothesis that streambed *K* would show greater statistical variability within an actively flowing stream channel environment relative to a compound bar structure, implying the dominance of deposition and erosion on *K* variability.

This experiment utilized the same methods employed in previous research to characterize streambed *K*, but as a repeated measures study targeted at differentiating between active processes. Densely sampled direct measurements of *K* utilizing hydraulic

methods act as the primary empirical data for hypothesis testing. Measurements of *K* in both approximately horizontal and vertical directions allow the characterization of anisotropy, and add to process understanding. Geophysical methods were used to record changes in streambed sedimentary structure that impact *K*. Grain size analyses of multiple sediment samples collected from where the hydraulic tests were conducted allowed for relevant changes in particle size affecting *K* to be identified. Changes in streambed geomorphology were recorded using aerial imagery from unmanned aircraft. Repeated measures ANOVA analyses were used to determine if changes in *K* between the same environment from different times were statistically significant as a quantitative means of hypothesis testing. Due to the labor intense nature of collecting such a comprehensive dataset, the temporal range of the study was limited to the summer season of 2017, lasting from June 2nd through August 3rd. As a result, this experiment is limited to differentiating between processes that control the short-term variability of streambed *K* heterogeneity.

CHAPTER 2.0 SITE DESCRIPTION

The field work for this research was completed on the Loup River approximately one kilometer downstream of the Loup River Genoa Headworks, near the city of Genoa, Nebraska. The Loup River Genoa Headworks is a canal diversion where water is diverted from the Loup River for hydroelectric power generation. The property is owned by the Loup Public Power District (LPPD) and field work was performed on their land with explicit oral permission. The entrance to the Genoa Headworks public access land is near the intersection of 350th and 530th streets in Nance County, Nebraska. The approximate latitude and longitude coordinates of the field site in decimal degrees are 41.391009 ; -97.812157.

2.1 Hydrology and Geomorphology

The Loup River at the study site is a perennial order 6 stream (USGS 2013) which begins approximately 8 km north of St. Paul, Nebraska at the confluence of the North and Middle Loup Rivers (figure 2-1). The drainage area of the Loup River calculated from the National Hydrography Dataset at the Genoa Headworks diversion is approximately 33,253.0 km^2, with a total length of stream in the drainage area of 25,183.55 km (Sniegocki and Langford 1959; Dingman 1978). The average length of overland flow (Horton's overland flow) through this drainage area is 0.66 km (Dingman 1978; USGS 2013). The western extent of the Loup's drainage area includes the Nebraska Sand Hills, which is an inactive, vegetated erg composed of well-sorted aeolian sands. The eastern extent of the drainage basin includes the dissected loess plains where the Loup erodes through Quaternary alluvium that contributes granite and feldspar gravel to the sediment load. From 1893 to 2017 Genoa received an average of 66.14 cm of

precipitation per year, with the majority of precipitation falling between the months of April and September (Sniegocki and Langford 1959; HPRCC 2017). A USGS gauging station (number 06793000) is located approximately 6.5 km downstream of the study area

Approximately 1 km upstream from the field site location, the LPPD diverts water from the Loup River for generating hydroelectric power. The volume of water diverted varies based on time of year and other factors, but the diversion can generally be assumed to be a considerable reduction in flow.

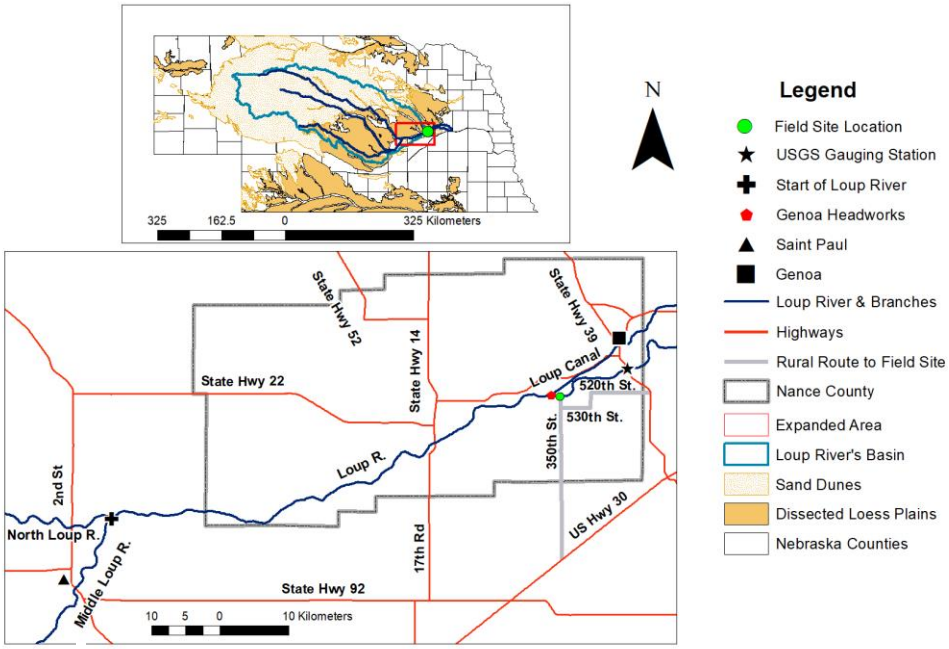

Figure 2-1: Location of field site within Nebraska.

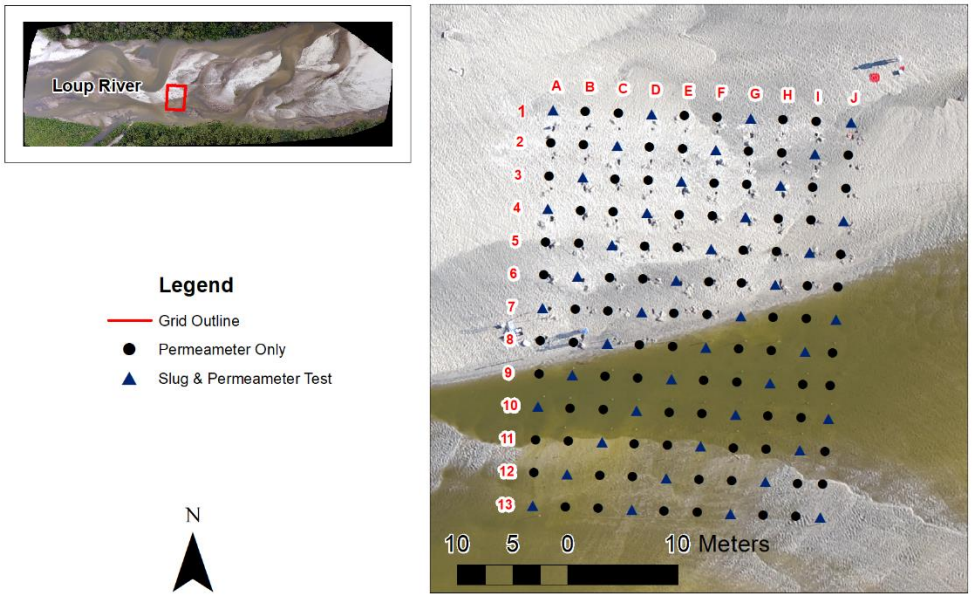

Figure 2-2: Map of the field site showing the locations of the hydraulic tests and their spatial sampling pattern.

The Loup River exhibits characteristics of both braided and meandering stream morphologies. The reach on which this study was conducted is straight for approximately 1 km with numerous composite braid bars. Upstream of the Genoa Headworks canal diversion there are more highly vegetated and thus more stable composite bars present. Downstream of the diversion the bars are considerably less vegetated and stable. There is a decrease in discharge on the Loup at the canal diversion, the decrease in discharge and stage causes more sand bars to be exposed downstream of the canal diversion. As can be seen in figure 2-1, a grid was developed within the Loup stream channel downstream of the diversion extending from a composite braid bar in the center of the channel into an actively flowing section of channel.

The width of the Loup River's floodplain at the site location is approximately 3.5 km. Sand dunes present in the area are part of a series of isolated dune fields associated with river valleys in east-central Nebraska. Despite the presence of small dunes, Genoa is not considered to be within the Sand Hills, but part of the Loess Hills region. Loess-topped hills are present within a few kilometers north of the field site.

2.2 Geology and Hydrogeology

Other than the 1959 USGS publication by Sniegocki and data from the Nebraska statewide test hole database, information on the geology and hydrogeology of the Genoa area is scarce. The Loup River alluvium at the field site is 3-4 meters thick and consists of 1-20% gravel by mass, 80-99% sand, and <1% silt, based on grain size analysis and GPR surveys performed during this study. The primary source of sediment for the Loup River is the Sand Hills, but gravel size clasts of granite, shale, and limestone come from Neogene and Quaternary deposits that underlie the aeolian deposits. These deposits consist of silt, sand, and gravel layers and are approximately 25 meters thick in this area (Table 2-1). The alluvium lies above Cretaceous bedrock which consists of calcareous shale and chalk from the Niobrara Formation.

The Loup River and the underlying Quaternary alluvium in this area represents a laterally continuous and productive unconfined aquifer (Sniegocki and Langford 1959). Discontinuous confining units are present locally, but there is no evidence of an underlying continuous confined aquifer (Sniegocki and Langford 1959). Agricultural irrigation wells can be observed within 2 km of the study site and are common throughout the Loup River floodplain and surrounding area.

System	Name	Lithology	Description	Depth (m)
Recent	Topsoil	Soil	silty, slightly clayey, sandy, brownish gray, sand is very fine to fine	0-0.3
	Loup River Alluvium	Silt	slightly clayey, very sandy, brownish gray	0.3-0.46
		Sand	very fine to fine, slightly silty from 0.46 to 0.73 m	0.46-1.52
		Sand & Gravel	fine with some medium, contains shale and limestone	1.52-3.05
		Gravel	fine to medium with coarse, contains shale and limestone	3.05-3.96
Quaternary	Quaternary Alluvium	Silt	slightly clayey, very sandy, dark gray to black, sand is very fine	3.96-4.11
		Silt	slightly clayey, brownish gray	4.11-4.27
		Silt	moderately clayey, moderately calcareous, medium brown, light brown below 5.79 m, contains limy areas below 4.57 m	4.27-7.32
		Silt	slightly to moderately clayey, medium brown, 7.62 m, slightly granular, slightly calcareous from 7.32 to 7.62 m,	7.32-13.72
		Silt	slightly clayey, moderately to very sandy, light brown, sand is very fine to medium below 14.54 m	13.72-15.24
		Silt	moderately to very clayey, slightly calcareous, brown, sand is very fine	15.24-16.31
		Sand	brownish gray, very fine to medium	16.31-16.76
		Sand	brownish gray, fine to medium with some coarse and a trace of very coarse	16.76-18.26
		Silt	moderately clayey, slightly sandy, light yellowish gray, very fine to medium sand	18.26-19.35
		Sand	very fine to fine with some medium, iron stained to 19.81 m	19.35-21.34
		Sand	brownish gray, fine to medium with some coarse and a trace of very coarse, contains thin silt layers from 22.1 to 22.22 m, and from 22.25 to 22.37 m	21.34-22.86
		Sand	brownish gray, medium to coarse with some very coarse, contains clay grains	22.86-24.38
		Sand	brownish gray, very fine to fine	24.38-27.37
		Silt	slightly clayey, very sandy, light yellowish gray	27.37-27.52
		Sand	brownish gray, fine to medium	27.52-28.65
		Sand & Gravel	brownish gray, very fine to medium, contains large amount of reworked shale, limestone, and clay grains	28.65-28.96
Cretaceous	Niobrara Formation	Shale	light olive gray, chalky, light gray from 29.57 to 29.72 m, light to medium gray from 29.72 to 33.53 m, medium gray below 33.53 m	28.96-39.62

Table 2-1: Logged geological data from Nebraska Conservation & Survey Division's 26-A-55 test hole located within 500 meters of the test grid.

CHAPTER 3.0 METHODS

3.1 Study Area Design

The study area for this research consisted of a rectangular grid 36 meters long by 27 meters wide in the Loup River streambed near the Genoa Headworks. The four corners of the grid were located relative to each other using a Brunton compass and measuring tape, and they were semi-permanently marked with tubes vibrated into the streambed. The grid consisted of 132 points separated by 3 meters of lateral distance from one another (figure 2-1). Approximately half of the grid was located on the immobile sand bar, and the other half was in the mobile channel sediments (figures 3-1 & 3-2). During each of the three data collection events, these points were marked with flags or stakes and GPS waypoints were taken at each location using a Trimble Geo7x handheld unit with an accuracy of ± 50 cm. The points comprising the grid were given alpha-numeric identifiers from column A to J, and rows 1 to 13, column A was the western most column and the northern most row was number 1. This test grid was not perfectly rectangular, with the two southern-most corners of the grid being almost 1 meter closer to each other than the northern most corners.

3.2 Slug Test Methodology

Characterizing *K* heterogeneity in streambeds is typically done by employing hydraulic methods that directly test the flow of water through the streambed sediments. The usefulness of slug testing for spatially characterizing *K* in streambeds has been demonstrated my multiple researchers (Bjerg et al. 1992; Cardenas and Zlotnik 2003a, 2003b; Conant 2004). Slug tests have the advantage of accurately characterizing streambed *K* in a small region around the well screen, but are disadvantaged by the fact

that they require high-accuracy pressure transducers to record subtle changes in water level. Operating such equipment in the streambed can be especially challenging. Slug tests also require that piezometers be installed in the streambed, which requires significant physical effort. Generally the *K* value resulting from a slug test is not given a directionality component, because, depending on the well geometry and aquifer properties some combination of vertical, horizontal, and oblique flow directions are always tested in the area surrounding the well screen (Zlotnik 1994).

The rate at which water level rises in a well after a slug of water is removed is given by (Bouwer and Rice 1976):

(2) $$\frac{dy}{dt} = \frac{-Q}{\pi r_c^2}$$

The Thiem equation can be modified to find the flow into a well:

(3) $$Q = 2\pi K L^* \frac{y}{\ln(R_e / r_w)}$$

Equations 2 and 3 are combined and integrated to give the following equation for *K*:

(4) $$K = \frac{r_c^2 \ln(R_e / r_w)}{2L^* t} \ln(\frac{y_0}{y_t})$$

Equation 4 allows *K* to be calculated from the recorded rise in water level after a rapid removal of a slug of water from a well after fitting a curve to the resulting straight line.

3.2.1 Slug Test Procedure

Temporary, hand-driven sand-point wells 5.08 cm in diameter were used to perform slug tests at 44 locations in the test grid. These wells had screen lengths of 30.48 cm and a mesh size of 60 (254 μm). Wells were driven into the streambed using standard fence post drivers (cylinder with two handles and one open end) until the bottom of the screen was 50 cm below the water-sediment interface. On the immobile braid bar, it was necessary to remove the unsaturated sand with a shovel until the water-sediment interface was reached. Immediately after emplacement of each well, the depth from the top of the well to the water level in the well was recorded using an electronic water level meter. During data collection, the total length of the well points was recorded at multiple times because the process of driving the wells into the streambed caused the upper rim of the well to curl in on itself, thus reducing the total length of the well. It was also necessary to periodically clean sediment out of the wells to ensure that the screen remained open and free.

Slug tests were completed at every 3rd point in the grid, starting at point A1 and working east toward column J in each row. In total, slug tests were performed at 44 points during each data collection event. A Solinst M5 water Levelogger© was used to record water pressure data during each slug test. The transducer was attached to a direct-read-cable connected to a radio-transmitter that allowed the logger to be started and stopped and for data to be downloaded using a cell phone. Water displacements (slug tests) in each well were performed using a bailer that was 4.06 cm in diameter and 30.48 cm long. After the bailer was deployed to its desired depth, it was allowed to sit still in the water for 20 seconds to allow the water level to adjust, after which time it was

removed and 1 minute was given for the water level to recover in the well. The slug test was repeated 3 times for each location.

Data processing was performed using Microsoft Excel and HydroSOLVE's AQTESOLV© software. Datalogger files were exported as Excel spreadsheets where drawdown and recovery data could be calculated for each slug test. While calculating drawdown and recovery in Excel, all late-time data with a drawdown <0.25 cm was deleted because the transducer used for these tests had an accuracy of +/- 0.25 cm. Recovery data was loaded into AQTESOLV from Excel and each curve was automatically matched to the Bouwer & Rice anisotropic recovery model. An anisotropy (K_h/K_v) value of 2 was used for all slug test processing. An AQTESOLV file was saved for each recovery curve, and the *K* value was recorded in an Excel spreadsheet. The average *K* resulting from the 3 slug tests performed at each location was accepted as the *K* value for a given location. For locations where the standard deviation of the 3 slug tests exceeded 7.0, the outlier value was excluded and the average of only 2 values was accepted. For a small minority of locations only 2 displacements were made and in these cases the values were always averaged. At a few locations, slug tests were repeated 4 times, so averages of 3 or 4 values were allowed for these cases depending on how many tests fell within the maximum standard deviation limit of 7.0. All *K* values were corrected to a temperature of 20^{o}C by converting *K* to intrinsic permeability (*k*), then back to *K*. The temperature of the water at each slug test location was recorded by the transducer. After the logger had sat in the well for several minutes the recorded temperatures generally stabilized around a single value. These temperatures were averaged to produce a single value representing the temperature of groundwater beneath

the braid bar and the stream channel, and these average values were used to correct all *K* data. This correction process was completed for each data collection event individually.

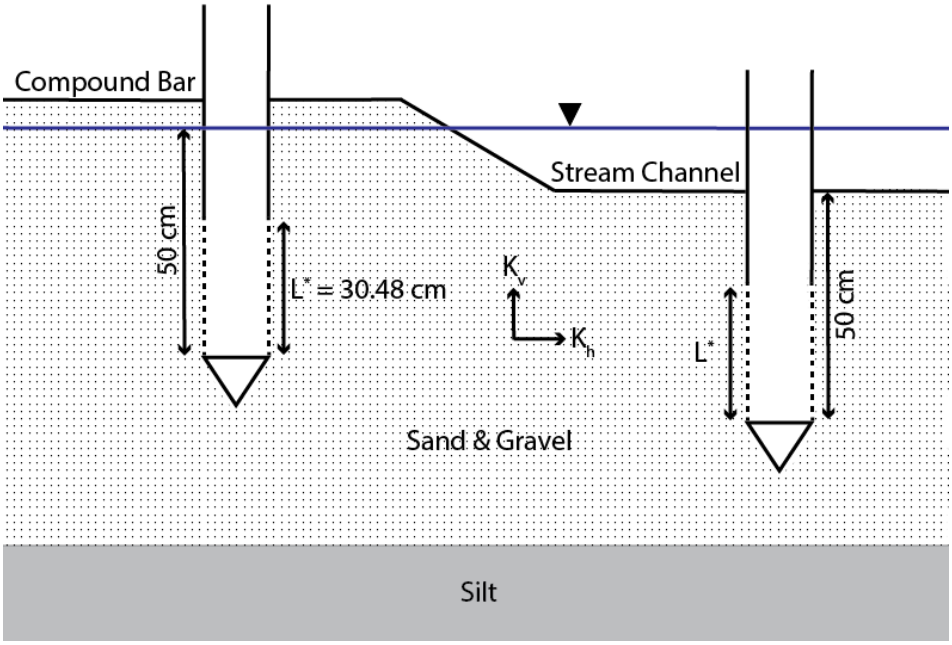

Figure 3-1: Diagram illustrating slug test methodology. Diagram is not to scale.

3.3 Falling Head Permeameter Methodology

Another commonly used method for characterizing *K* in streambeds is known as the falling head permeameter test, or simply permeameter. The permeameter test generally involves inserting a clear plastic tube into the streambed sediments and filling it with water, then recording the drop in head in intervals (Landon et al. 2001). The permeameter is a preferred method for researchers working in the streambed because of quick instillation and testing times as well as ease of data processing (Chen 2000; Genereux et al. 2008; Dong et al. 2012; Jiang et al. 2015; Sebok et al. 2015). The permeameter test differs from the slug test in that the sediment tested is contained within the tube, and water can be forced through the sediments in a reliably vertical direction,

meaning that K_v can be calculated as an isolated variable (Chen 2000). Permeameters have been used to explore the anisotropy of streambed deposits by orienting the tubes in both the standard vertical, and in horizontal directions (Chen 2000).

From a falling head permeameter test, the drop in water level can determine K_v using the following equation (Hvorslev 1951.):

$$(5)\quad K_v = \frac{\frac{\pi}{11}\frac{D}{m} + L}{t_1 - t_0} \ln\left(\frac{H_0}{H_1}\right)$$

3.3.1 Falling Head Permeameter Procedure

At each of the 132 points located within the test grid, a falling head permeameter test was conducted to determine K_v. Tests were performed using plastic tubes that are 152.3 cm long with a diameter of 4.5 cm. Tubes were emplaced in the streambed to a depth of 50 cm from the bottom of each tube to the sediment water interface using the Specialty Devices Incorporated VibeCore mini© to reduce sediment compaction. Tubes were filled to their top with water from the Loup River and the head drop was recorded using a clipboard and stopwatch. The time was recorded after each 0.5 cm drop in head, and 10 head-time measurements were taken at each test location. At sites where K_v was low, less than 10 measurements were sometimes taken for the sake of time efficiency. After each permeameter test was completed, the tube was capped to create suction so that the sediments within the tube could be removed from the streambed for sieve analysis.

Permeameter data was processed by entering the recorded head-time data into a Microsoft Excel spreadsheet (Xun Hong Chen, personal communication) that calculates K_v by using linear estimation (LINEST function in Excel). The program assumes that

there is a linear relationship between the change in head gradient and the shape factor, the time interval, and the hydraulic conductivity of the sediments. The product of the change in head gradients and the shape factor are considered the known y values, the time intervals over which head dropped are considered the known x values, and the LINEST function returns an *m* value which in this case is K_v. For the purpose of these calculations the LINEST function is told to force the b value to be zero. This method of calculating K_v from permeameter data reduces error by taking all 10 measurements into account simultaneously. An anisotropy (K_h/K_v) value of 2 was used for all permeameter data processing (Chen 2004). K_v data were corrected to a temperature of 20°C by converting K_v to intrinsic permeability, then back to K_v using 20°C as the water temperature. The temperature of the water was not recorded at each permeameter location, rather an average temperature

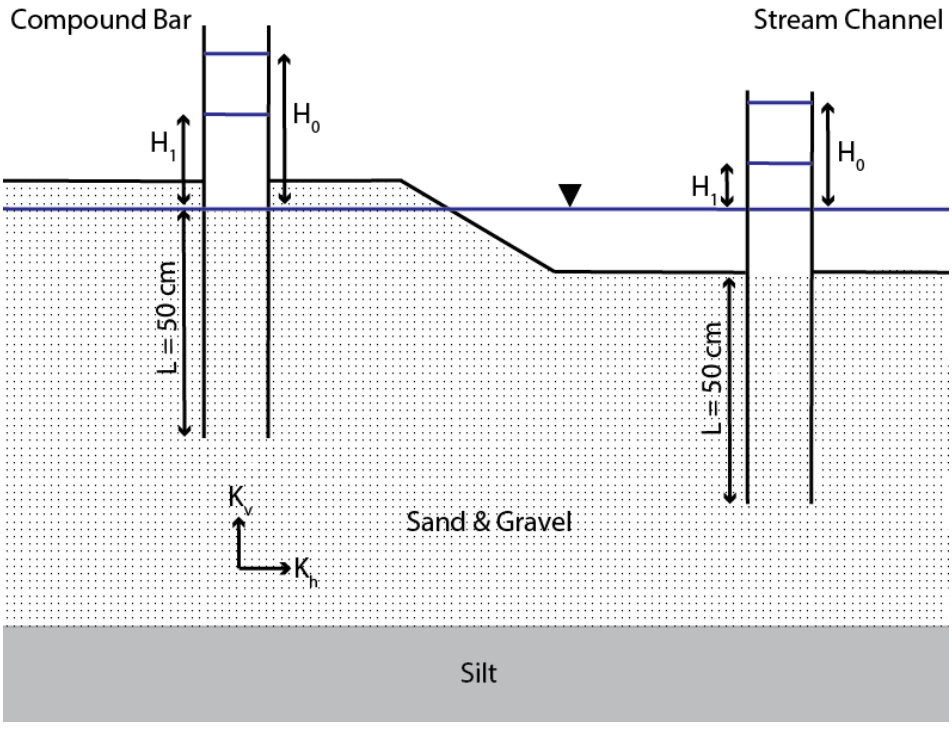

Figure 3-2: Diagram illustrating permeameter methodology. Diagram not to scale.

for the immobile and mobile environments were determine from slug test transducer data for each collection event.

3.4 Geophysics Methodology

Geophysical methods are sometimes employed by hydrogeologists for the purpose of imaging aquifer geometry and structure, as well as for investigating sites with groundwater contamination (Rubin and Hubbard 2006). Ground penetrating radar (GPR) and frequency domain electromagnetic (EM) surveys have specifically been used for aquifer heterogeneity characterization (Kirsch 2009). Both of these methods have significant limitations when it comes to hydrogeological applications, but in the right circumstances and in combination with other data, they can be valuable tools (Kirsch 2009).

EM surveys utilize two coils separated by a fixed distance, one alternating current coil to generate and transmit an electromagnetic field into the subsurface, and another coil to receive the induced electromagnetic fields produced by subsurface materials (Rubin and Hubbard 2006). The strength of the measured induced currents can be used to infer the electrical conductivity of the subsurface materials within the depth of penetration, which itself is largely controlled by the electrical properties of the subsurface. Depth of penetration is a significant limiting factor for the application of EM to hydrogeological problems. The depth of penetration of EM surveys ranges from 0.75 to 1.5 times the coil separation distance. For ground-based EM surveys, the coil separation distance is often less or much less than 5 meters, meaning that with ideal subsurface electrical properties depth of penetration would be limited to less than 7.5 meters.

Ground based EM surveys are rarely carried out for hydrogeological investigations, with airborne surveys being preferred because of their greater depth of penetration and greater coverage area (Kirsch 2009). Burrell et al. (2007) used ground based EM surveys to characterize the sedimentary architecture of ephemeral streams in the southern high plains of Texas. This research demonstrated that EM data can be used to suggest the locations of sedimentary structures within streambeds, especially when high resolution EM equipment was used (Burrell et al. 2008).

GPR is a complex technology that utilizes a transmitting antenna to propagate microwave band electromagnetic radiation into the subsurface, where changes in the electrical properties of Earth materials create reflections that are recorded by a receiving antenna (Jol 2009). GPRs produce high resolution images of the subsurface response to microwave radiation, not an exact image of the subsurface itself. GPR signals are extremely susceptible to attenuation from high electrical permittivity materials such as clays and brines, which makes GPR limited in terms of hydrogeological investigations. GPR depth of penetration is inversely proportional to the center frequency of the transmitting antenna, but is also significantly affected by the electrical properties of the subsurface materials. Dry sand and ice are among the most ideal Earth materials upon which GPR surveys can be conducted.

Several articles have been published that apply GPR in sandy streambeds to explore the sedimentology and stratigraphy of fluvial deposits. Mumpy et al (2007) utilized 3D GPR surveys to image the architecture of an active braid bar on the Wisconsin River. A 225 MHz GPR antenna was used to complete a grid of 16 survey lines across an entire mid channel braid bar, the resulting 2D cross sections were

combined into a fence-post diagram where interpreted structures could be tracked in 3D (Mumpy et al. 2007). Burrell et al. (2007) utilized GPR to complement their EM investigations of ephemeral stream deposits in Texas. When completed prior to GPR surveys, they showed that EM data could be a powerful predictive tool for where to collect GPR data to image streambed structure. It was demonstrated that antennas of different center frequencies could fill different roles, with the high frequency antennas imaging fine structures such as cross beds, whereas lower frequency antennas imaged the sub-channel structure and possible paleo-channels (Burrell et al. 2008). Cardenas & Zlotnik (2003a) combined GPR surveys with multilevel slug testing, constant head injection, and multilevel grain size analysis to produce a 3D model of *K* heterogeneity in Prairie Creek, Nebraska. Consistent reflectors observed in GPR data were interpreted as a scour surface which corresponded well to kriged isolines at 10, 15, and 20 meters per day (m/d) of *K*.

3.4.1 Ground Penetrating Radar Procedure

Ground penetrating radar (GPR) was used to image the near-subsurface structure of the Loup River streambed and to confirm aquifer thickness. A Mala GroundExplorer High Dynamic Range© was used with a 450 MHz antenna to take images along lines down each column and row of the rectangular test grid. This was accomplished both on the immobile bar and the stream channel itself by loading the GPR antenna into an inflatable raft that could be dragged along the sand and float in water. It was necessary to use a time interval triggering function built into the GPR unit to record reflected microwave signals because the triggering wheel could not be used with the antenna in a raft.

GPR data was processed using MATGPR 3.1 (Tzanis 2006). The processing steps taken for this data started with picking the time of first signal detection as time zero, "DWOW," performing an inverse amplitude decay of order 4, and a band pass filter centered around 450 MHz. The last four steps of this process were completed as a "batch job" in the MATGPR software. Lines that were collected using automatic triggering were converted to equal spacing using "rubber band interpolation" or "rubber sheeting" from marker data collected in the field. Hyperbola matching was performed on multiple lines to determine a reasonable average velocity for the subsurface. A velocity of 0.055 m/ns was used to transform time to depth. No topography correction was attempted because the streambed was very nearly horizontal for all collected lines.

3.4.2 Frequency Domain Electromagnetics Procedure

Frequency domain electromagnetic geophysical surveys were performed with a GSSI Profiler EMP 400 while using a Trimble Geo7x handheld GPS as the control unit. Frequencies of 1500, 3000, and 8000 hertz were used for data collection. Data was recorded in continuous mode with a vertical dipole moment induction orientation. The instrument was calibrated to the operating height of the person carrying the device for each survey, as well as calibrated to set the in-phase value to zero. Due to the ease with which electromagnetic data can be collected, the survey area was expanded to include the entire compound bar as seen in figure 2-1. Surveys began at the west end of the bar and lines were walked in a "zig-zag" fashion in the north-south direction until the east end of the bar had been reached.

3.5 Sediment Particle Size Analysis Methodology

K can be empirically determined using the grain size distribution curve of the sediments of interest. In the streambed, grain size analysis has been used alongside direct hydraulic methods for determining *K* (Landon et al. 2001; Cardenas and Zlotnik 2003a). Landon et al (2001) reported that empirically derived *K* from grain size using the Hazen (1880) and Alyamani & Sen (1993) equations was generally lower than *K* determined by hydraulic tests. Cardenas & Zlotnik (2003) demonstrated a strong correlation between *K* derived from grain size and both slug tests and constant head injection tests, with the Terzaghi (1925) formula providing a particularly strong correlation. Generally, *K* derived from grain size distribution is not considered as reliable as direct hydraulic tests for determining *K* (Landon et al. 2001).

3.5.1 Sediment Particle Size Analysis Procedure

The sediments tested for K_v in each permeameter were collected for particle size analysis via sieving. Samples were collected in bags after lifting each capped permeameter tube out of the streambed. In the laboratory, samples were sieved using 8, 4, 2, 1, 0.833, 0.5, 0.25, 0.088, and 0.063 mm sieves. All sieving was completed using an automatic sieve vibrating machine for two minutes to ensure thorough separation. Grain size distribution curves and statistics were calculated using the Excel calculator "Gradistatv8" (Blott and Pye 2001).

K was empirically calculated from grain size distributions using two different models: 1. Hazen 2. Seelheim. For the Hazen method a "c" empirical coefficient of 150 was used implying that d_{10} was in units of centimeters. For the Seelheim method an empirical coefficient of 0.00357 was used. Grain size diameters were taken from the

Gradistatv8 Excel calculator. For this research, the Hazen equation was used in the following form (Hazen 1893):

(6) $K = cd_{10}^2$

The Seelheim equation is given by (Seelheim 1880):

(7) $K = 0.00357 d_{50}^2$

3.6 Aerial Imagery Methodology

A DJI Phantom 4 Quadcopter was used to collect aerial imagery of the field site. A pre-programmed flight path was used to ensure the entire field area was covered consistently in each flight and to maintain an appropriate amount of overlap between successive images. Black and white targets were placed in the field as ground control targets with logged GPR coordinates for georeferencing. Orthophotos were created using Pix4D© software by generating a point cloud and georeferencing using the ground control targets. Minor georeferencing adjustments were made by aligning all orthophotos with ground control targets from 7/17/2017 for accuracy and warping corrections.

3.7 Repeated Measures Analysis Methodology

ANOVA or “analysis of variance” can be described as a means for identifying the causes of variability between recorded datasets (Girden 2017). ANOVA can also be described as a way of determining if the variability between means of different datasets is great enough that it is improbable that it is due to random chance. ANOVA is one of the primary techniques by which empirical relationships between phenomena are asserted (Girden 2017). The standard one-way ANOVA consists of an independent variable and a dependent variable, where the independent variable is categorical, and the dependent

variable is continuous. (Lund Research 2013). An ANOVA can be considered an expansion of Student's t-test, which is a method of determining the equality of means between two random datasets. To apply a basic ANOVA, the following assumptions must be met:

1. Independence – The datasets being compared need to be randomly sampled so that there is no relationship between them that could account for the tested variance (Diez 2015).
2. Normality – The datasets being compared must follow an *approximate* normal distribution (Diez 2015). ANOVA tests hold up to some partial violation of the normality assumption, especially when no extreme outliers are present in the datasets. The normality assumption is especially important when the datasets being tested are small.
3. Constant Variance – The variance of the tested datasets must be approximately the same, with some minor variability being acceptable (Diez 2015).

A repeated measures analysis is a variation of a standard one-way ANOVA for datasets that are *not* independent from one another, violating the first assumption listed above (Lund Research 2013). Repeated measures analyses can be used to test the differences between means from datasets collected at three or more different times, or means from datasets collected during three or more different situations (Lund Research 2013). Repeated measures analysis uses a technique to remove the variability between the test subjects from the total variability, thus leaving only the variability due to changes in conditions between datasets (Lund Research 2013).

The inter-subject variability is accounted for by determining the covariance structure of the datasets being tested (Lipka and Tyner 2004). Put in plain language, covariance structures are patterns that describe the between-subjects variability (Lipka and Tyner 2004). Many covariance structures exist and typically an AICc is used to select the structure most appropriate for the datasets being tested. An AICc is a version of an AIC which stands for "Akaike Information Criterion," which is a statistical estimator that determines the fitness of a statistical model relative to other models (Hu 1987; Giraud 2014).

The covariance structure with the lowest AICc for a particular dataset is considered the model of best fit (Hu 1987). It is important to note that AIC's and AICc's are not hypothesis tests, and also can only describe which model fits best *relative* to other models (Hu 1987).

The null hypothesis of a repeated measures analysis is that the means of the tested datasets are not significantly different from one another. This hypothesis is either accepted or rejected based on the resulting p-value, which can be calculated at a desired confidence interval.

3.7.1 Repeated Measures Analysis Procedure

The statistical software "Statistical Analysis System" or "SAS" was used to perform all statistical calculations and tests for this research, as well as to produce several plots. Aerial imagery combined with field notes taken during the experiment were used to classify K/K_v data as belonging to the immobile compound bar, or the mobile stream channel environments. The raw data were then compiled into an Excel spread sheet where K/K_v values from different times at each point were stacked with each other. The points

E8, D8, and G7 were excluded from the final analysis because these points changed environment during the experiment which introduces variability into the statistical tests that is not relevant for hypothesis testing in this study.

SAS was initially used to calculate AICc values for different covariance structures to eliminate inter-subject variability arising from the dependent nature of this time series data. The covariance structures that were compared in SAS are: unstructured (UN), compound symmetry (CS), heterogenous autoregressive (ARH(1)), first-order autoregressive (AR(1)), and ante-dependence: first order (ANTE(1)). The covariance structure with the lowest AICc was used to perform the repeated measures analysis.

Four separate analyses were used to compare K/K_v data collected at each of the three data collection events (times) from each environment. Explicitly, a repeated measures analysis between the three data collection events was performed for: K_v data collected from the mobile environment, K_v collected from the immobile environment, K collected from the mobile environment, and K collected from the immobile environment. Each of the four repeated measures analyses were calculated with an independently determined covariance structure across the three time points. P-values were calculated at the 95% confidence interval such that p-values of less than 0.05 indicated rejection of the null hypothesis.

CHAPTER 4.0 RESULTS

4.1 Aerial Imagery and Streambed Evolution

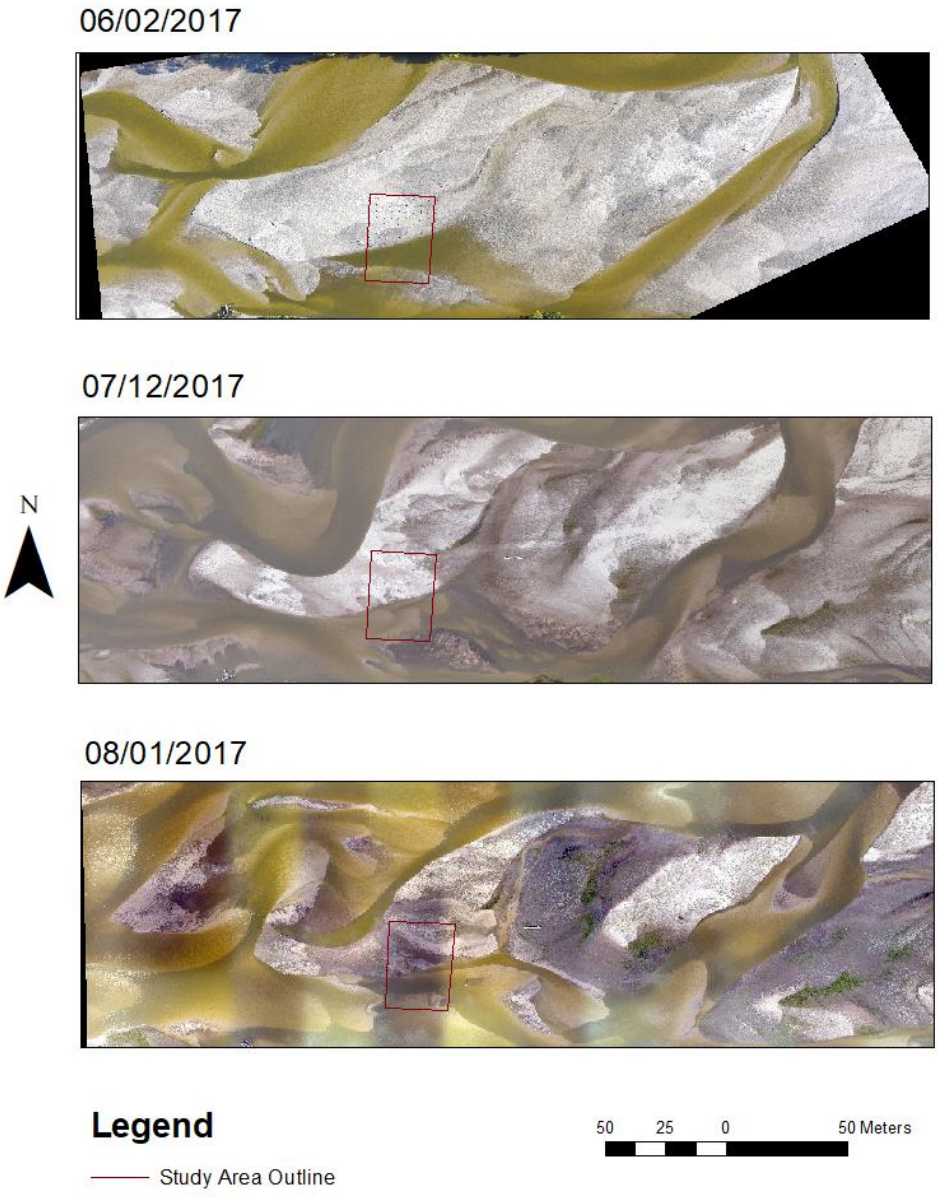

Figure 4-1: Aerial imagery of the study site taken from a drone on three different dates during the summer of 2017.

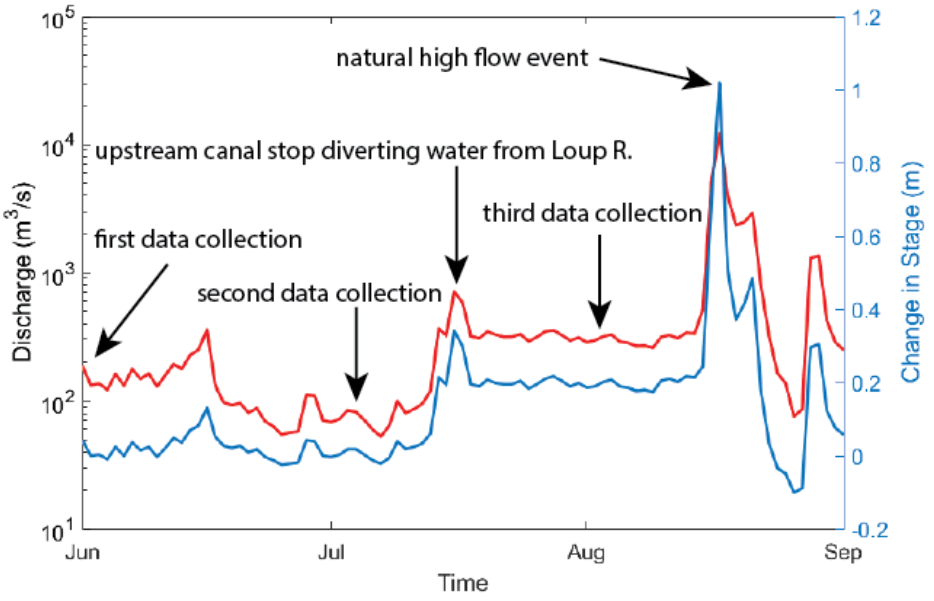

Figure 4-2: Hydrograph from the USGS gauging station near Genoa, NE showing discharge and change in stage relative to 6/02/2017 near the field site on the Loup river from 6/02/2017 to 9/01/2017.

The boundary between active channel and compound bar within the study area remained consistent throughout the study period. This stability is important because it allowed the statistical analysis of the data to compare variability between the two environments without reclassification of point measurements. In other ways, the streambed experienced geomorphic and hydrologic changes during the study period. Figure 4-1 shows that between 7/05/2017 and 8/03/2017 a prominent channel was eroded into the immobile (compound bar) portion of the study area. Outside of the study area, figure 4-1 shows morphological changes to the streambed such as the expansion of the point bar – cut bank system immediately to the northwest of the study area. It is also apparent that the exposed bar sediments got progressively darker over the study period. Field observations indicate that a thin layer of organic-rich mud was deposited on the bar between 7/15/2017 and 8/03/2017. Green patches seen in the image from 8/03/2017 are new grass, indicating that the bar sediments were biologically active.

On 7/15/2017, nineteen days before the third data collection event, U.S. Federal Energy Regulation Commission (FERC) regulations forced the Loup Public Power District to briefly stop diverting water from the Loup River with their canal located approximately 1 km upstream from the field site (Ellyson 2017). It was reported by Tyler Ellyson of the Columbus Telegram that on 7/17/2017 the FERC granted the power district a waiver to resume water diversion. This resulted in a 90% increase in discharge recorded by the USGS stream gauge near Genoa, NE between 7/07/2017 and 7/15/2017 (figure 4-2). Figure 4-2 also shows that discharge remained consistently high after this increase, indicating that it is possible that the FERC waiver allowing water diversion to resume was conditional and did not allow the power district to resume operations fully.

Figure 4-2 shows changes in stage downstream of the study area at a USGS gauging station. Stage was not appreciably different on 6/02/2017 and 7/05/2017, while stage had increased by approximately 20 cm between 7/05/2017 and 8/03/2017. These observations are important because an increase in stage changes the location of the sediment-water interface, which was the reference used to position the permeameters and piezometers, but only on the compound bar environment. Data from the stream channel would be unaffected by increases in stage because the location of the sediment-water interface does not necessarily change in response. It should also be noted that the USGS stream gauge from which this data was acquired is located 6.5 km downstream of the study site where discharge may not be identical to conditions at the field site.

4.2 *K*-Data

4.2.1 Slug Test Results

Parameter	All Slug Tests (m/d)	06/02/2017 Immobile (m/d)	06/02/2017 Mobile (m/d)	07/05/2017 Immobile (m/d)	07/05/2017 Mobile (m/d)	08/03/2017 Immobile (m/d)	08/03/2017 Mobile (m/d)
Test Count	132.00	24	20	24	20	24	20
Mean	22.76	21.84	27.57	21.28	26.86	17.21	23.10
Maximum	53.20	35.34	53.20	31.48	33.89	32.50	34.92
Minimum	10.09	15.52	20.35	12.27	17.06	10.09	12.80
Standard Deviation	6.26	4.48	6.82	5.17	4.10	5.41	5.43
Range	43.11	19.82	32.85	19.20	16.83	22.40	22.12

Table 4-1: Descriptive statistics from all slug tests "*K*."

In tables 4-2 through 4-4, *K* values from slug tests are reported in a pseudo-spatially oriented grid. Bold values represent *K* from the mobile stream channel, while values in regular font are from the immobile compound bar. The alpha-numeric name of each point can be found by following the top row of the table and the far-left column. Blank cells represent data points where slug tests were not conducted. All units are in meters per day.

	A	B	C	D	E	F	G	H	I	J
1	22.21			28.51			35.34			22.40
2			24.52			17.37			16.66	
3		24.00			19.73			17.83		
4	19.40			17.65			21.25			17.24
5			15.52			20.55			20.19	
6		22.29			23.84			18.15		
7	23.60			22.72			26.39			***30.60***
8			26.78			***29.09***			***53.20***	
9		***27.84***			***35.23***			***27.79***		
10	***22.55***			***24.51***			***26.80***			***25.11***
11			***27.61***			***26.67***			***26.31***	
12		***27.14***			***24.27***			***24.97***		
13	***23.08***			***24.20***			***24.11***			***20.35***

Table 4-2: *K* values from slug tests completed during the first collection event on 6/02/17.

	A	B	C	D	E	F	G	H	I	J
1	21.32			27.72			24.72			24.83
2			25.45			17.82			19.82	
3		18.61			15.86			12.27		
4	15.52			15.73			17.56			17.13
5			17.17			27.44			22.89	
6		20.50			31.17			18.27		
7	21.91			31.48			***25.87***			***27.71***
8			24.12			***24.99***			***27.58***	
9		***33.75***			***30.88***			***24.72***		
10	***17.06***			***18.15***			***28.04***			***26.83***
11			***30.29***			***26.70***			***26.75***	
12		***30.85***			***25.29***			***27.04***		
13	***24.16***			***33.89***			***27.84***			***25.61***

Table 4-3: *K* values from slug tests completed during the second collection event on 7/05/2017.

	A	B	C	D	E	F	G	H	I	j
1	18.44			15.69			32.50			12.91
2			15.09			10.92			10.09	
3		20.56			18.52			13.46		
4	16.94			12.28			15.53			15.63
5			11.72			18.80			14.75	
6		17.06			19.71			14.19		
7	17.76			20.38			18.74			***18.58***
8			31.36			***22.35***			***17.59***	
9		***29.58***			***34.92***			***24.82***		
10	***12.80***			***17.38***			***25.05***			***25.48***
11			***32.45***			***22.93***			***22.41***	
12		***29.19***			***19.57***			***21.32***		
13	***21.64***			***23.52***			***23.10***			***17.39***

Table 4-4: *K* values from slug tests completed during the third collection event on 8/03/2017.

4.2.2 Falling Head Permeameter Test Results

Parameter	All Permeameter Tests (m/d)	06/02/2017 Immobile (m/d)	06/02/2017 Mobile (m/d)	07/05/2017 Immobile (m/d)	07/05/2017 Mobile (m/d)	08/03/2017 Immobile (m/d)	08/03/2017 Mobile (m/d)
Test Count	390.00	72	58	72	58	72	58
Mean	19.85	22.58	15.06	25.31	19.11	18.40	17.40
Maximum	43.88	35.45	31.82	38.37	43.88	30.64	30.77
Minimum	0.54	5.91	2.07	2.07	0.54	1.56	0.78
Standard Deviation	8.92	0.77	1.05	0.88	1.50	0.78	1.18
Range	43.34	29.54	29.75	36.30	43.34	29.07	29.99

Table 4-5: Table 4-1: Descriptive statistics from all permeameter tests "K_v" and each collection event.

In tables 4-6 through 4-8, K_v values from permeameter tests are reported in a pseudo-spatially oriented grid. Bold values represent K_v values from the mobile stream channel, while values in regular font are from the immobile compound bar. The alpha-numeric name of each point can be found by following the top row of the table and the far-left column. All units are in meters per day.

	A	B	C	D	E	F	G	H	I	J
1	21.39	21.77	25.31	29.71	23.59	25.33	29.63	29.61	21.92	22.60
2	33.36	23.50	20.89	5.91	26.78	21.44	12.14	11.12	6.12	13.20
3	23.95	32.03	32.77	20.39	25.22	15.67	15.16	12.50	11.18	14.64
4	19.19	16.81	20.02	14.18	26.11	21.14	22.31	27.56	27.26	20.22
5	17.74	17.31	15.73	18.42	18.19	29.24	29.35	30.56	23.70	23.69
6	19.08	22.76	30.42	27.50	28.71	22.31	19.43	16.35	24.70	24.64
7	21.23	29.08	30.92	32.21	25.49	19.04	23.10	***20.18***	***20.81***	***10.32***
8	34.34	35.45	23.53	26.19	21.97	***6.47***	***15.17***	***14.57***	***13.24***	***11.28***
9	***18.76***	***17.30***	***10.72***	***4.66***	***4.28***	***7.09***	***9.57***	***17.61***	***17.82***	***5.14***
10	***3.68***	***2.97***	***2.07***	***17.92***	***10.21***	***11.57***	***16.00***	***7.52***	***13.25***	***6.69***
11	***10.72***	***6.52***	***7.43***	***10.60***	***11.58***	***10.90***	***6.46***	***9.32***	***9.70***	***8.79***
12	***18.82***	***22.93***	***22.55***	***23.83***	***19.71***	***20.63***	***26.56***	***20.92***	***9.01***	***8.58***
13	***22.28***	***25.08***	***28.52***	***24.49***	***28.43***	***31.82***	***24.08***	***29.86***	***30.69***	***25.55***

Table 4-6: K_v values from permeameter tests completed during the first collection event on 6/02/2017.

	A	B	C	D	E	F	G	H	I	J
1	22.32	26.75	28.97	36.25	25.01	29.21	28.07	26.71	27.53	20.12
2	33.46	32.68	16.67	26.88	29.78	29.48	14.24	12.83	16.57	17.31
3	2.07	27.06	36.92	23.68	24.31	18.12	15.18	19.41	14.74	21.63
4	22.32	18.68	11.66	15.47	32.38	24.27	13.65	35.93	26.78	21.58
5	16.92	19.43	18.89	24.26	21.97	33.67	34.86	26.55	24.73	26.95
6	21.69	27.13	30.13	26.56	33.32	30.32	38.37	25.01	29.69	28.44
7	21.50	32.52	35.07	32.63	30.18	25.76	***22.72***	***21.86***	***5.59***	**2.48**
8	36.40	34.78	32.16	***33.37***	***23.41***	***19.53***	***2.68***	***22.73***	***21.08***	**6.81**
9	***28.53***	***22.87***	***25.87***	***3.80***	***20.84***	***12.63***	***13.43***	***26.49***	***4.36***	**0.54**
10	***6.34***	***7.50***	***6.13***	***2.76***	***31.20***	***3.37***	***4.37***	***1.54***	***1.92***	**1.37**
11	***6.62***	***26.76***	***28.21***	***28.84***	***24.49***	***5.55***	***5.42***	***23.14***	***7.60***	**28.42**
12	***31.02***	***32.87***	***33.31***	***25.32***	***21.23***	***28.63***	***28.73***	***27.84***	***30.00***	**27.31**
13	***15.71***	***32.48***	***18.35***	***31.00***	***31.94***	***28.61***	***39.26***	***28.72***	***43.88***	**16.02**

Table 4-7: K_v values from permeameter tests completed during the second collection event on 7/05/2017.

	A	B	C	D	E	F	G	H	I	J
1	13.77	19.96	20.52	26.46	16.33	27.28	19.54	21.32	17.83	6.64
2	16.14	25.11	23.10	23.96	20.67	15.60	12.87	12.55	16.47	15.65
3	19.15	24.86	24.26	22.04	19.41	18.43	21.82	14.52	3.74	17.89
4	18.54	6.43	13.08	17.26	20.43	25.57	27.92	26.64	23.78	28.18
5	17.13	13.27	9.96	8.25	14.49	17.47	17.01	23.96	23.94	21.64
6	19.74	23.97	25.41	28.25	18.86	25.44	2.17	11.32	12.16	13.71
7	18.72	20.82	19.72	21.76	23.06	18.54	***21.14***	**11.31**	**5.30**	**1.85**
8	30.64	1.56	15.58	3.96	**5.61**	**22.10**	**6.75**	**0.80**	**15.21**	**27.00**
9	***18.95***	***10.15***	***15.97***	***6.09***	***16.48***	***6.78***	***15.43***	***20.11***	***25.02***	***9.51***
10	***3.84***	***4.36***	***4.03***	***0.78***	***23.41***	***29.99***	***16.06***	***22.05***	***25.69***	***18.62***
11	***17.55***	***21.68***	***21.13***	***29.34***	***30.06***	***3.04***	***29.03***	***21.74***	***3.55***	***11.07***
12	***30.77***	***27.25***	***29.69***	***27.72***	***26.63***	***28.41***	***22.66***	***25.05***	***13.37***	***13.36***
13	***3.69***	***27.55***	***23.94***	***16.27***	***27.90***	***22.55***	***23.73***	***20.08***	***19.94***	***14.73***

Table 4-8: K_v values from permeameter tests completed during the third collection event on 8/03/2017

2.2.3 K Data Visualization

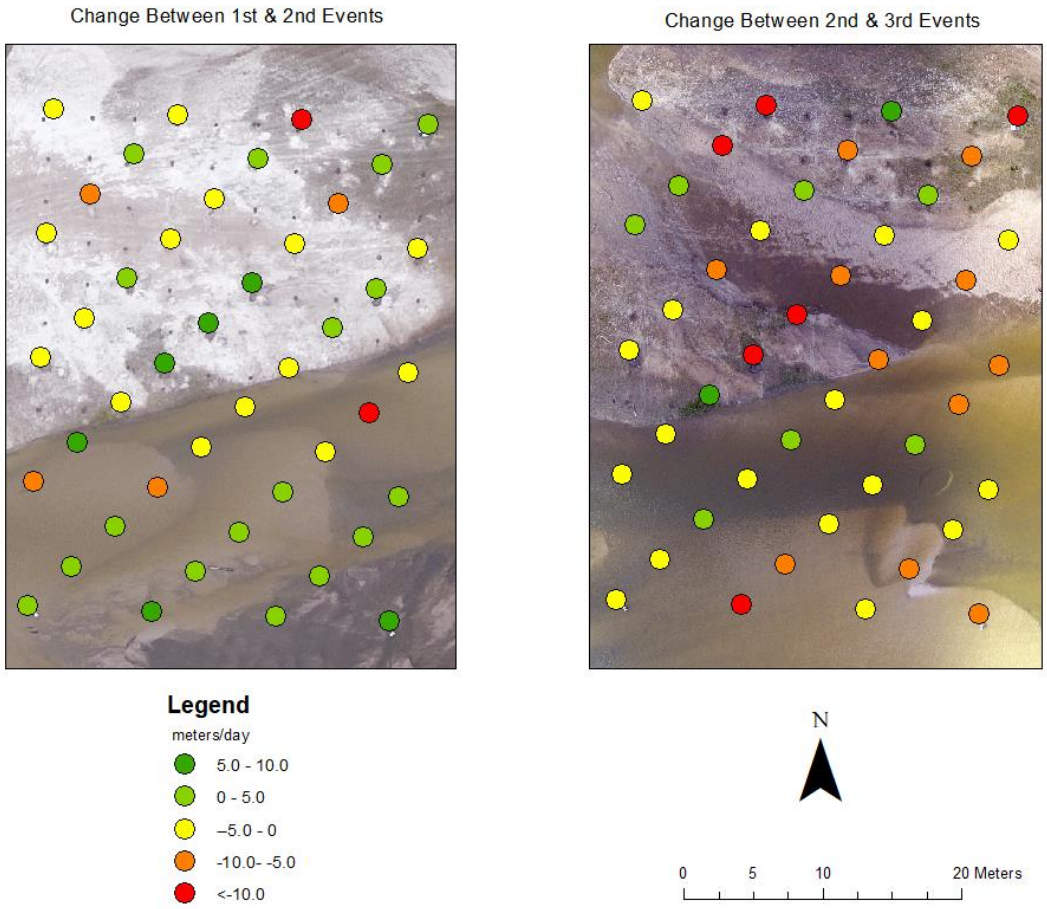

Figure 4-3: Visualized changes in slug test *K*. Image on the left shows the changes between 6/02/2017 and 7/05/2017. Image on the right shows the changes between 7/05/2017 and 8/03/2017. Background images are aerial imagery collected 7/05/2017 (left) and 8/01/2017 (right).

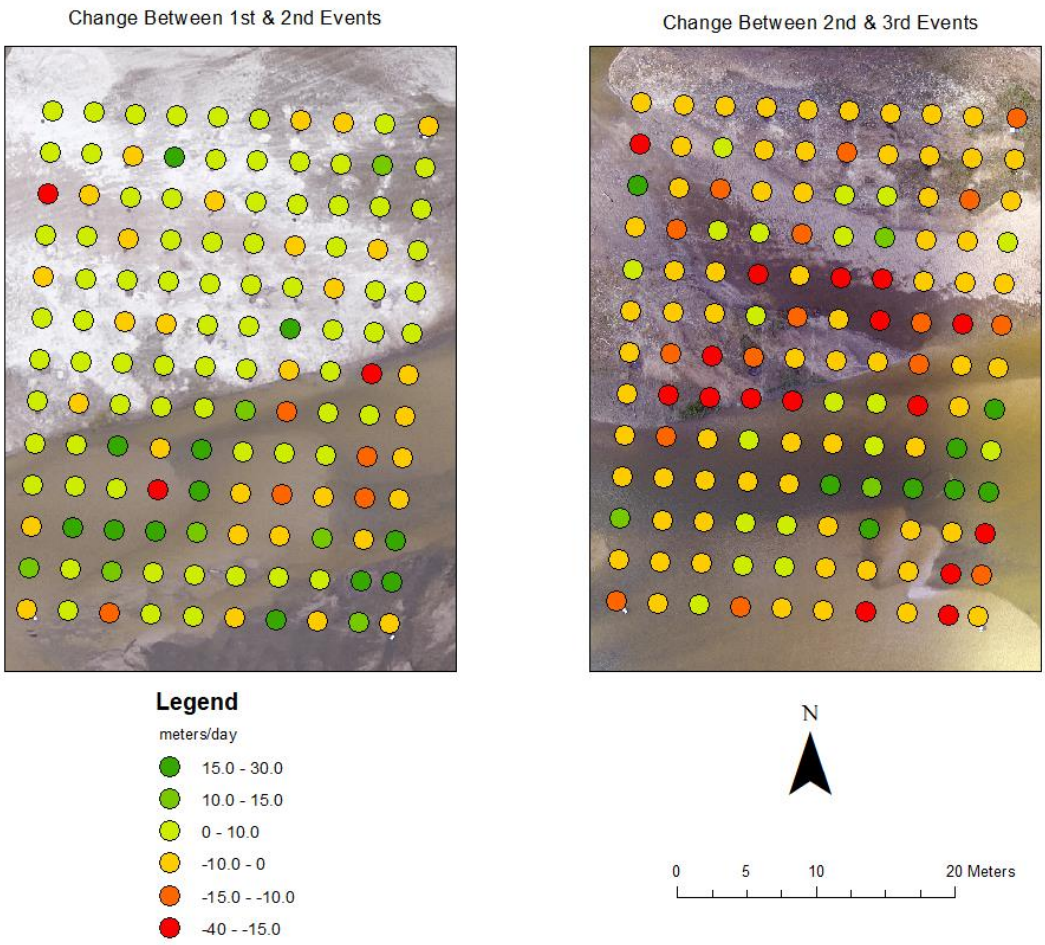

Figure 4-4: Visualized changes in permeameter K_v. Image on the left shows the changes between 6/02/2017 and 7/05/2017. Image on the right shows the changes between 7/05/2017 and 8/03/2017. Background images are aerial imagery collected 7/05/2017 (left) and 8/01/2017 (right).

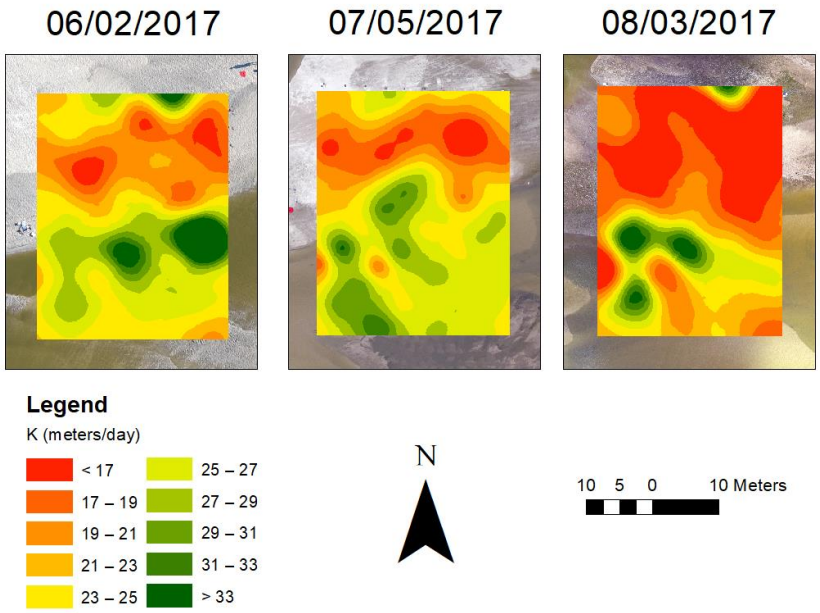

Figure 4-5: Kriged surface of slug test *K* from each data collection event. Aerial drone images are shown in the background.

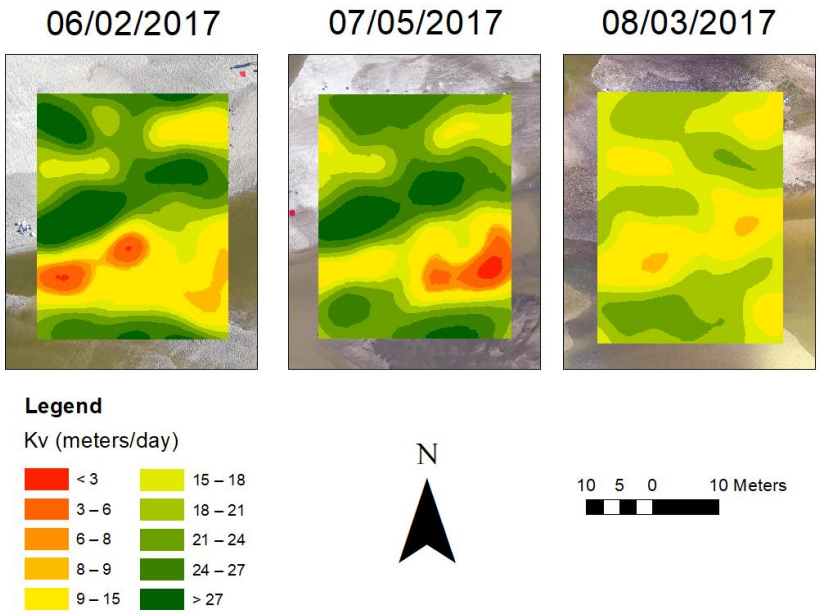

Figure 4-6: Kriged surface of K_v data from each data collection event. Aerial drone images are shown in the background.

Tables 4-1 and 4-5 show descriptive summary statistics for K and K_v from all data collection events. Tables 4-1 through 4-8 and figures 4-5 and 4-6 show clear spatial patterns in the K and K_v data. K_v was generally higher on the compound bar than in the stream channel. In the northeast corner of the stream channel (not the whole grid) K_v was lowest with values of less than 1 meter per day. In the field, it was observed that silt was actively being deposited in this part of the channel because the channel widens and deepens in this location. Thin silt layers that restrict flow in the vertical direction are likely responsible for the low K_v in this area. The maximum K value was 0.21% greater than the maximum K_v value, while the minimum K value was 17.7% greater than the minimum K_v value (tables 4-1 and 4-5). The difference between minimum K and K_v values implies that anisotropy was present in the streambed sediments. Most of the anisotropy was located in the stream channel, shown in figure 4-6 where interpolated K_v values are lowest throughout all data collection events. Table 4-1 shows that average K decreased by approximately 2% between 6/02/2017 and 7/05/2017, but decreased approximately 17% between 7/05/2017 and 8/03/2017. Table 4-5 shows that average K_v increased approximately 16.5% between 6/02/2017 and 7/05/2017, and decreased approximately 20% between 7/05/2017 and 8/03/2017. These same trends are illustrated in figures 4-3 through 4-6.

4.3 Geophysics Results

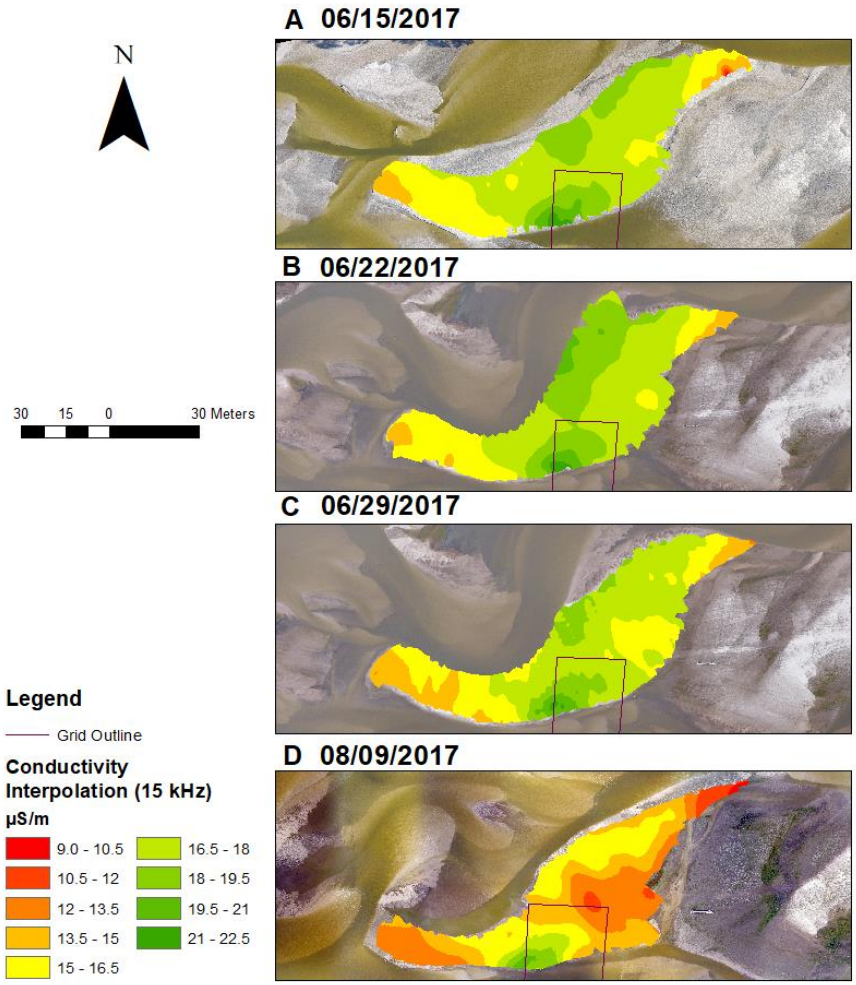

Figure 4-7: Kriged surfaces of the electrical conductivity changes over time of the compound bar in the study area.

Two separate GPR surveys were conducted on 7/12/2017 and 8/01/2017 to record changes in streambed subsurface structure. During each survey, 23 lines of GPR data were collected along the rows and columns of the test grid, but only select lines that illustrate major features and changes are presented here.

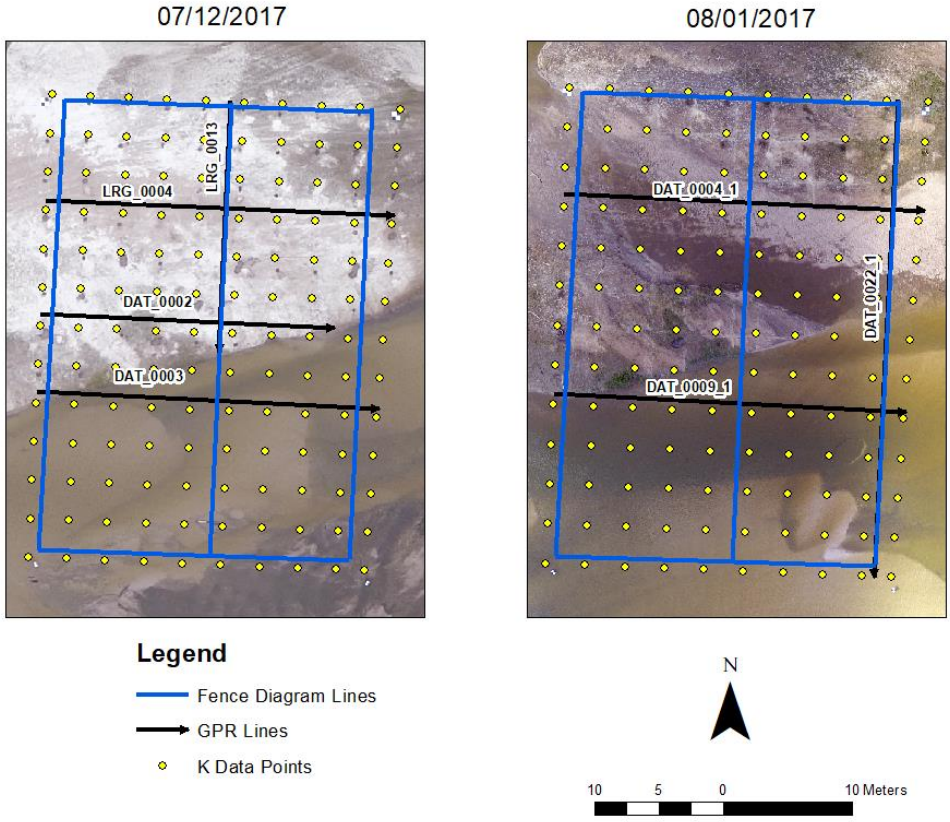

Figure 4-8: Approximate locations on the study grid of GPR lines in figures 4-9 through 4-15. Note that GPR lines were shot between each row and column of the study grid, but only select lines are reported here.

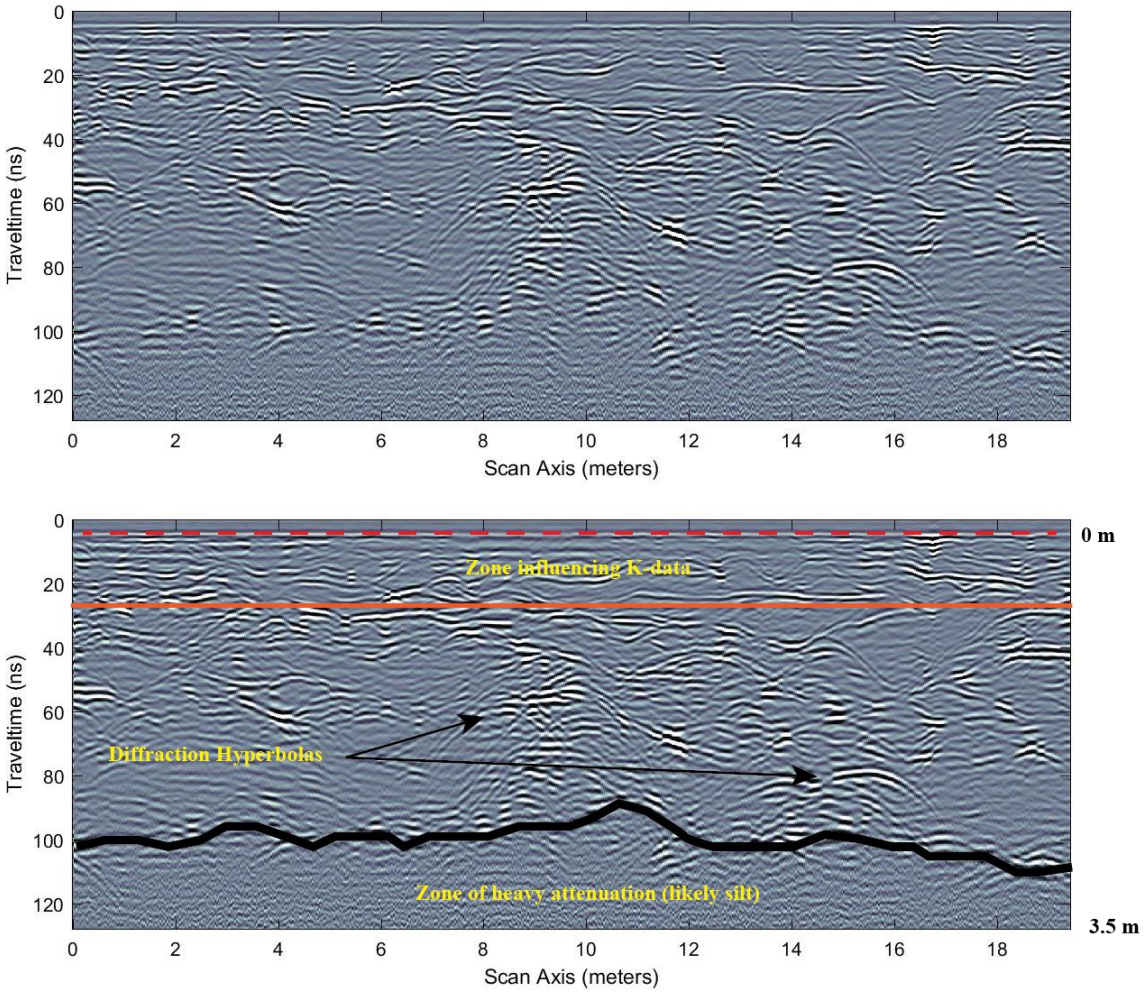

Figure 4-9: GPR line LRG_0013 taken on the immobile compound bar on 7/12/2017. The top image is uninterpreted, whereas the bottom is interpreted. The dashed red line represents the sediment-water interface, whereas the heavy black line represents the interpreted base of active alluvium and the transition from sand & gravel to silt. Most linear and dipping features in the profile are interpreted as sedimentary structures such as bedding planes in sand.

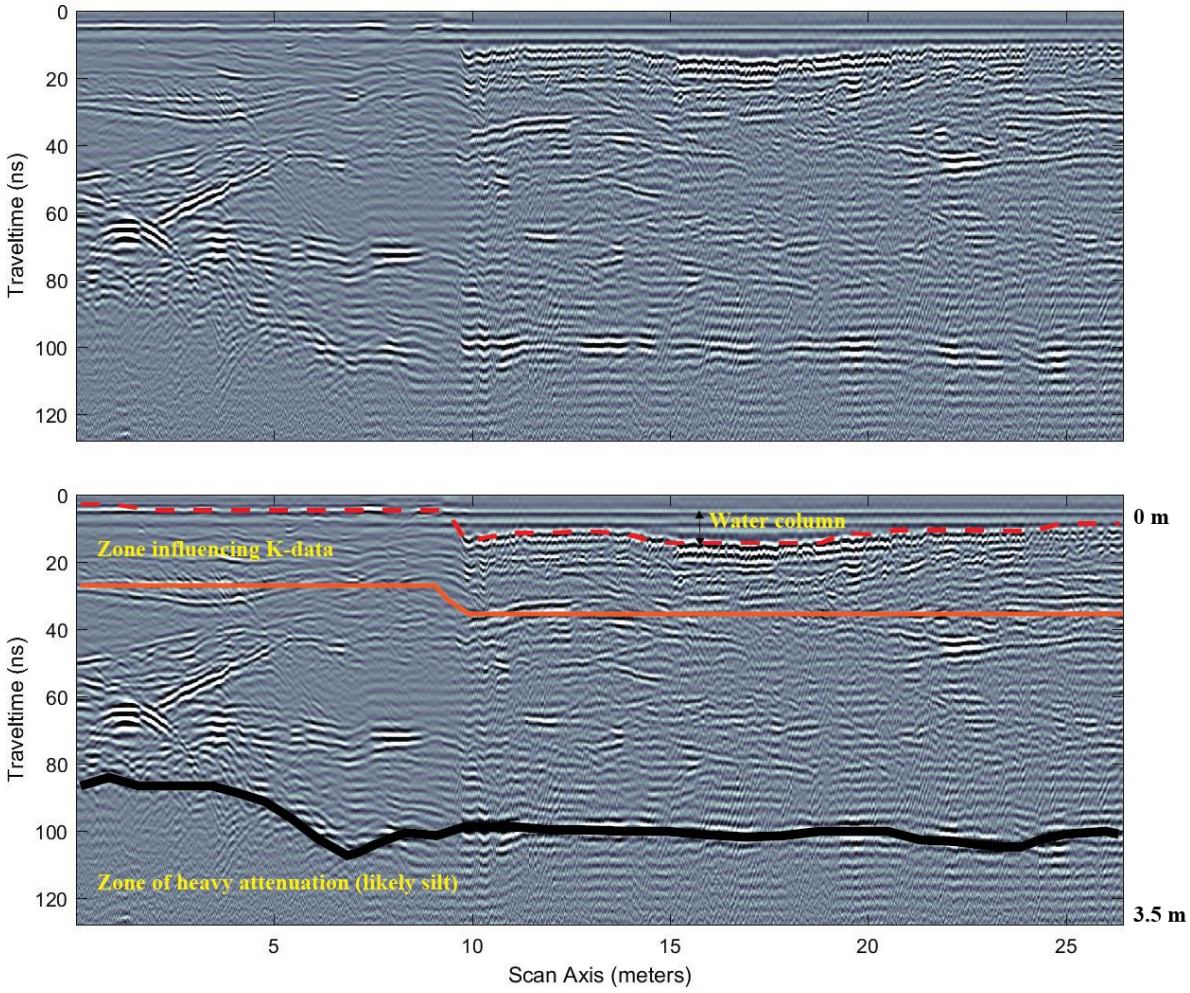

Figure 4-10: GPR line DAT_0002 from 7/12/2017 that includes both compound bar & stream channel environments. The top image is uninterpreted, whereas the bottom is interpreted. The dashed red line represents the sediment water interface, whereas the heavy black line represents the base of active alluvium. Note the transition from bar to channel where the "kink" in the sediment water interface is located, left of the image's middle.

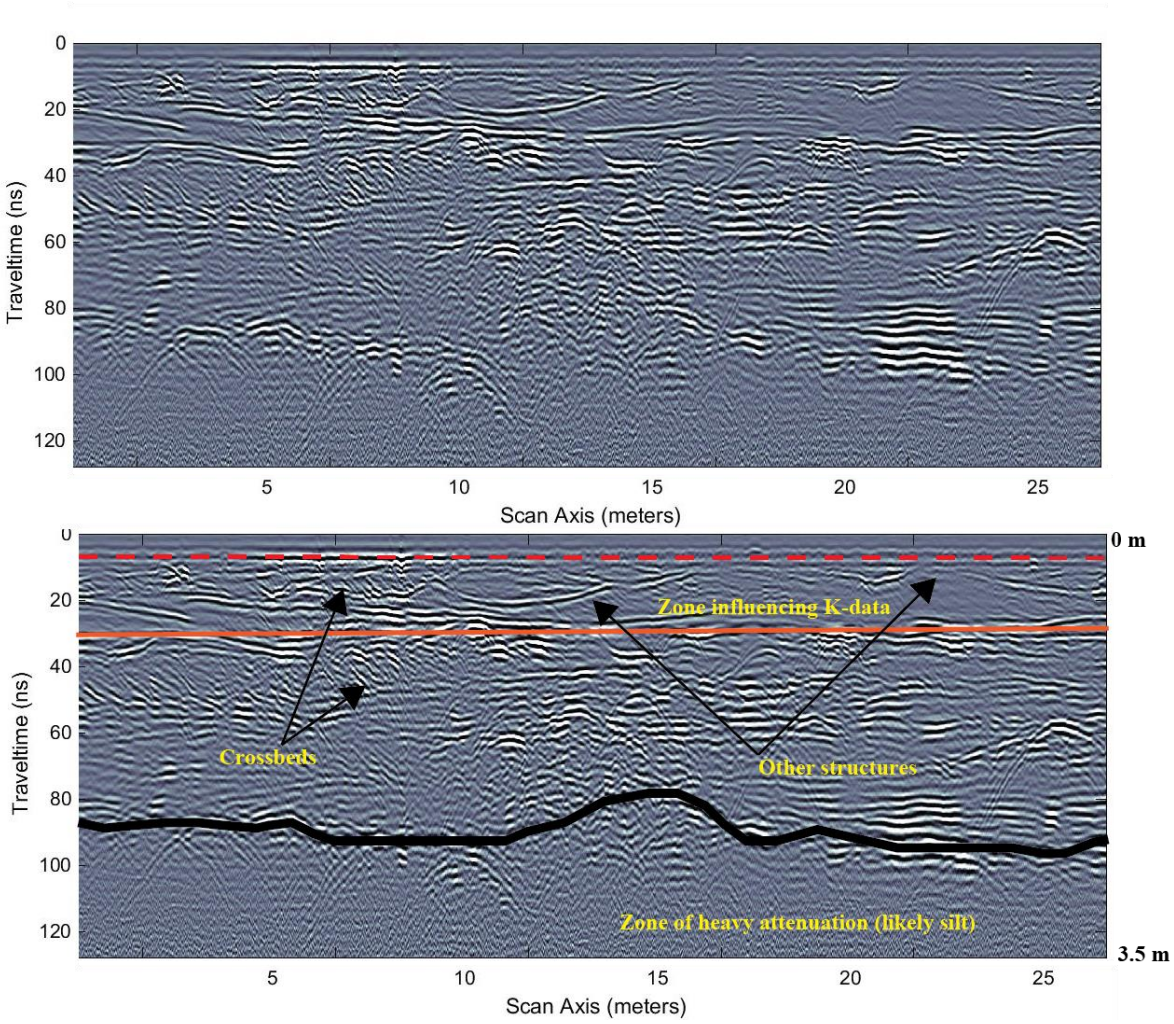

Figure 4-11: GPR line DAT_0004_1 from 8/01/2017. This profile only shows the compound bar. The top image is uninterpreted, whereas bottom is interpreted. Red dashed line represents the sediment water interface, whereas the heavy black line represents the base of active alluvium.

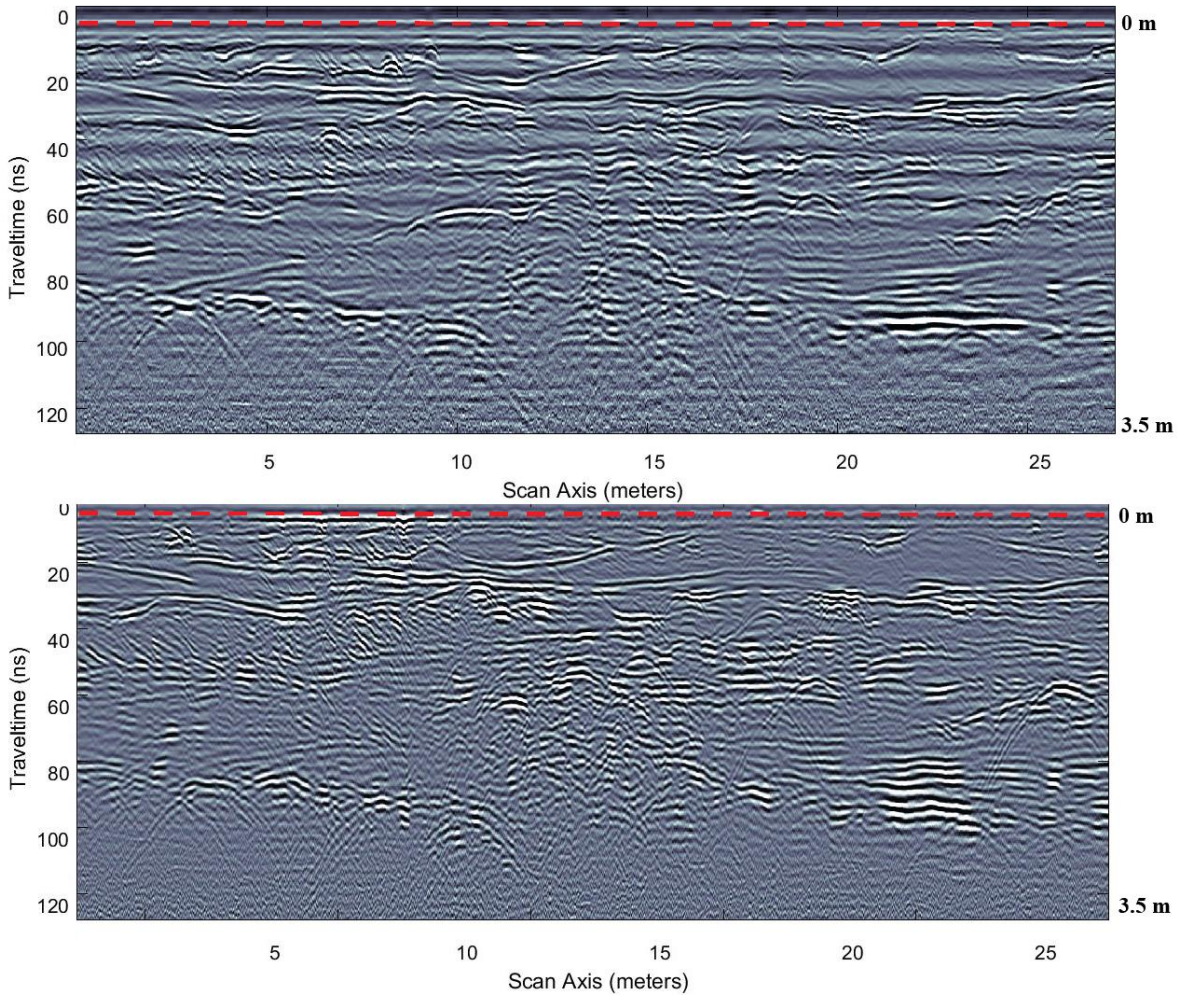

Figure 4-12: The top image is line LRG_0004 from 7/12/2017, the bottom image is line DAT_0004_1 from 8/01/2017. These two profiles were collected from approximately the same location. The red dashed line represents the sediment water interface.

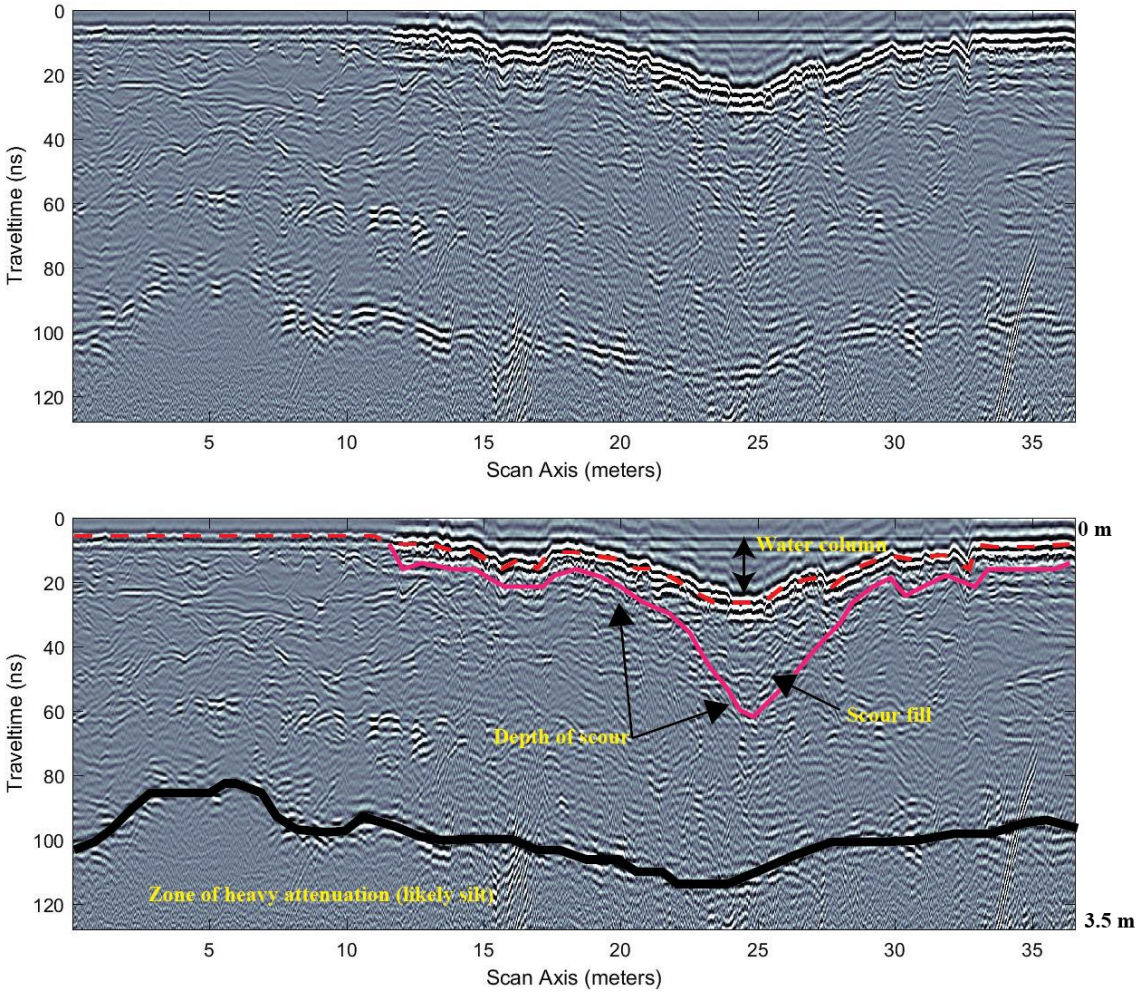

Figure 4-13: GPR line DAT_0022_1 from 8/01/2017. This profile documents a transition from compound bar to stream channel. The red dashed line represents the sediment-water interface, whereas the heavy black line represents the base of active alluvium. The direction of flowing water would be into the page.

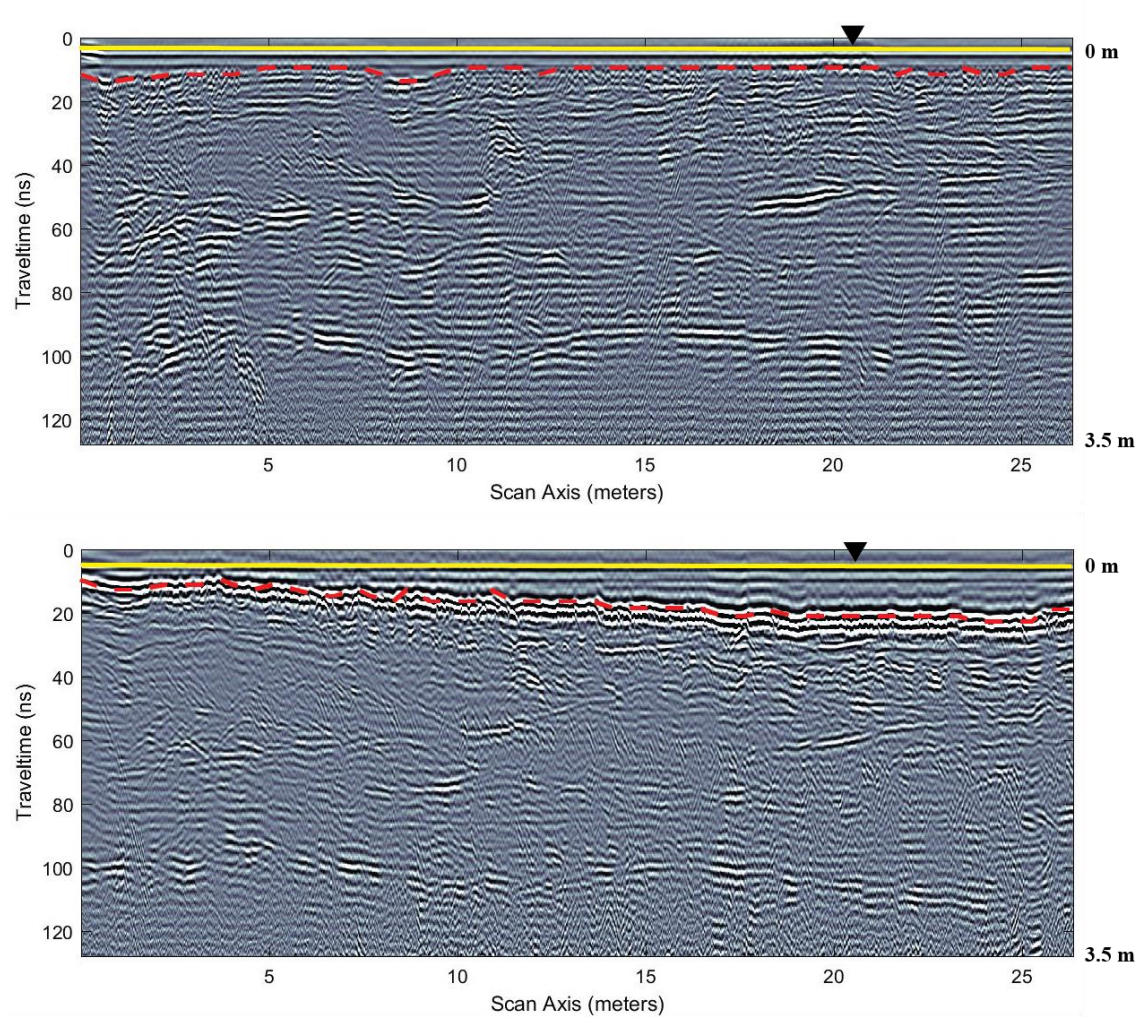

Figure 4-14: The top image is line DAT_0003 from 7/12/2017, the bottom image is line DAT_0009_1 from 8/01/2017. These two profiles were collected over approximately the same location in the mobile stream channel. The red dashed line represents the sediment-water interface, whereas the solid yellow lines represents the water surface of the river. Note changes in bathymetry over time by analyzing differences in the sediment-water interface between the two profiles.

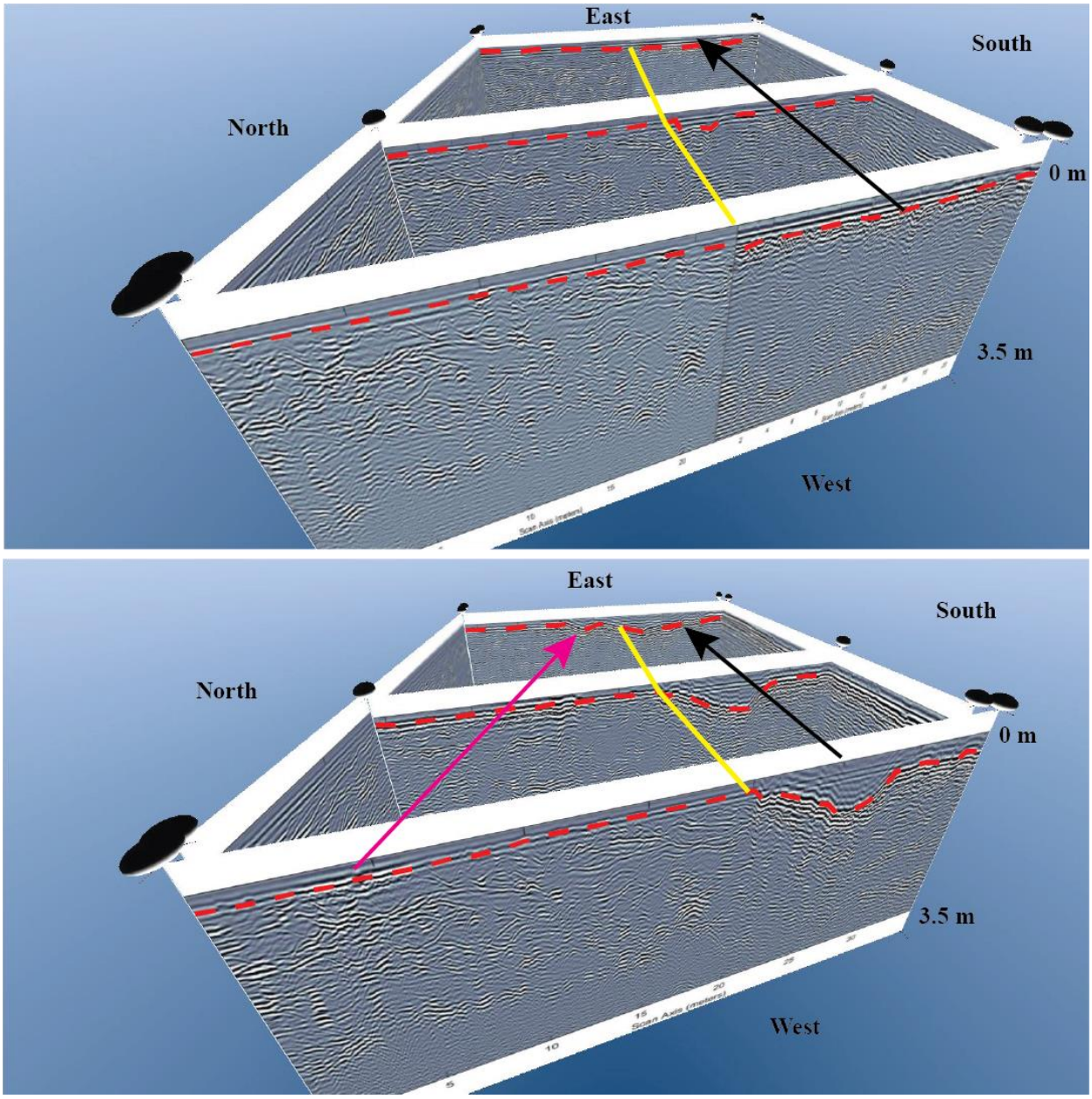

Figure 4-15: Fence diagram comparing GPR profiles collected from approximately the same locations on the gird. The top image is from 7/12/2017 while the bottom image is from 8/01/2017. The red dashed lines represent the sediment-water interface, the yellow lines represent the boundary between compound bar and the main stream channel, black arrows represent flow direction in the main stream channel, and the magenta arrow represents the location of the small channel formed atop the compound bar between the second and third data collection events.

Figure 4-7 shows the changes in electrical conductivity of the compound bar over time. Average electrical conductivity increased 1.3% between 6/15/2017 and 6/22/2017, decreased 3.8% between 6/22/2017 and 6/29/2017, and decreased 13.2% between panes 6/29/2017 and 8/09/2017. The reduction in electrical conductivity between 6/29/17 and 8/09/17, after the mid-July increase in discharge, mimics decreases in *K* recorded by hydraulic tests.

Figure 4-9 is a GPR profile displaying diffraction hyperbolas used to calculate an average velocity of GPR signals in the streambed. The depth of the sediment water interface in figures 4-9 through 4-15 is based on field observations made during hydraulic testing, but its actual depth in the images cannot be accurately known because of obfuscation by the ground and air waves which are located at the ground-atmosphere interface. The base of the bar and zone of heavy attenuation correlates well with silt logged at 4 meters in test hole 26-A-55 shown in table 2-1. This test hole log and the fact that this feature appears in all recorded GPR profiles at approximately the same depth is evidence that the feature is laterally continuous, at least within the streambed. It should be noted that no cores were taken within the study area to explicitly confirm this interpretation due to the costs and risk to equipment associated with doing so.

Figure 4-10 illustrates the difference in quality between GPR data collected on the compound bar and data collected in the flowing stream channel. In figure 4-10, the boundary between the channel and the bar can clearly be tracked as a vertical line through the image that was created by increased noise introduced by the signal passing through water. It should be noted that in figures 4-10, 4-13, 4-14, and 4-15 that include data from the stream channel, the presence of water reduces the velocity of GPR signals

passing through it relative to data collected on the bar. It is apparent from examining figures 4-10 and 4-13 that this retardation of signal velocity did not have an effect on the recorded data because laterally continuous features can be tracked at the same depth within these profiles. In figure 4-13 the interpreted base of alluvium appears to track the deepest water in the channel above, which could be a manifestation of signal velocity retardation.

Figure 4-11 highlights the range of sedimentary structures that can be interpreted from the collected GPR data. Parallel dipping reflectors in the upper left of the image are interpreted as cross bedding. Flat-lying reflectors present in figure 4-11, as well as all other profiles, likely represent bedding planes without dip. Figure 4-11 contains arrows pointing to "other structures," these features are difficult to interpret but are prominent and intriguing. It is possible that they represent trough cross bedding, cross sections of unit bars, or preserved dunes. These interpretations are difficult to confirm from a GPR profile, but it is interpreted that these reflectors represent non-linear sedimentary structures within the compound bar.

Figure 4-12 demonstrates that between 7/12/2017 and 8/01/2017, no appreciable changes in sedimentary structure occurred on the compound bar portion of the test grid. The same interpreted sedimentary structures can be seen in both GPR profiles collected over approximately the same location. This observation is salient because the hypothesis of this research is dependent on comparing two stable streambed environments. Figure 4-15 also shows compound bar stability across multiple profiles, and directly contrasts this stability with the recorded changes from the stream channel environment.

Figures 4-13, 4-14, and 4-15 are important because they record evidence of deposition and erosion between 7/05/2017 and 8/03/2017. Figure 4-13 includes a surface that is interpreted to be the depth of scour achieved during the high flow event caused by the cessation of water diversion by the upstream canal. Above the interpreted depth of scour surface are parallel reflectors that track both the depth of scour and the channel bathymetry. These features are interpreted to be sequences of erosion and deposition that partially filled the scoured channel. If this interpretation is correct then GPR suggests that the stream channel was scoured to a depth of over 1 meter below the previous sediment water interface between 7/05/2017 and 8/03/2017. Figures 4-14 and 4-15 exhibit more straightforward evidence for erosion between the final data collection events because they show profiles from 7/05/2017 compared to those from 8/03/2017 collected at approximately the same locations. Figure 4-14 shows a clear increase in channel depth as well as what is interpreted to be the same scour surface from figure 4-13, but shown parallel to flow. Figure 4-15 shows, in three dimensions, the extent to which the major stream channel was incised between 7/05/2017 and 8/03/2017, providing clear evidence that deposition and erosion occurred during that time.

4.4 Grain Size Results

	Data Collection Event:	6/02/2017	7/05/2017	8/03/2017
Average	Initial Weight (g)	1122.46	1357.87	1373.00
Average Percent Mass Retained in Each Sieve	8000 (µm)	0.39	0.36	0.23
	4000 (µm)	0.92	0.90	0.72
	2000 (µm)	1.66	1.62	1.37
	1000 (µm)	3.11	2.93	2.49
	833 (µm)	1.24	1.08	0.93
	500 (µm)	34.59	57.58	53.12
	250 (µm)	52.35	30.89	35.03
	150 (µm)	4.30	2.77	4.52
	125 (µm)	0.70	0.51	0.67
	88 (µm)	0.43	0.40	0.54
	63 (µm)	0.13	0.19	0.24
	<63 (µm)	0.04	0.10	0.12
Average	d_{10} (µm)	269.20	306.75	295.30
	Sorting (folk & ward, µm)	1.61	1.54	1.54

Table 4-9: Results of grain size analysis. Data are averages from all 130 processed samples from each data collection event.

Event	6/02/2017	7/05/2017	8/03/2017
Immobile Bar Fine Fraction (grams)	0.5	0.5	1.1
Mobile Channel Fine Fraction (grams)	0.4	2.2	2.3
Average Sample Mass (grams)	1122.46	1357.87	1373.00

Table 4-10: Changes in fine fraction (<63 µm) recorded from each environment and data collection event.

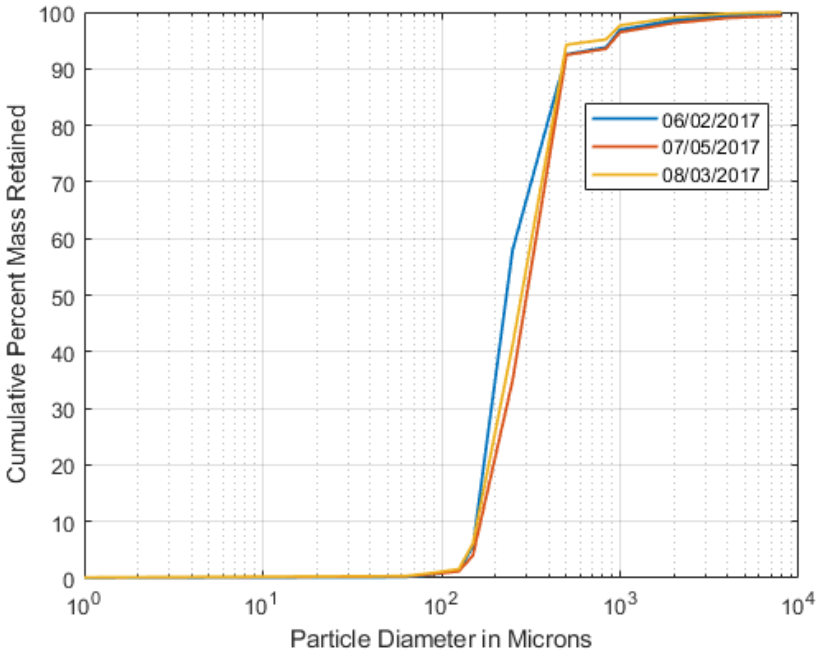

Figure 4-16: Cumulative frequency diagram of the average mass retained through sieving from samples collected during each data collection event.

In figures 4-17 through 4-19, point location numbers refer to slug test locations as follows: A1 equals point 1, B3, equals point 5, J13 equals point 44, and so on.

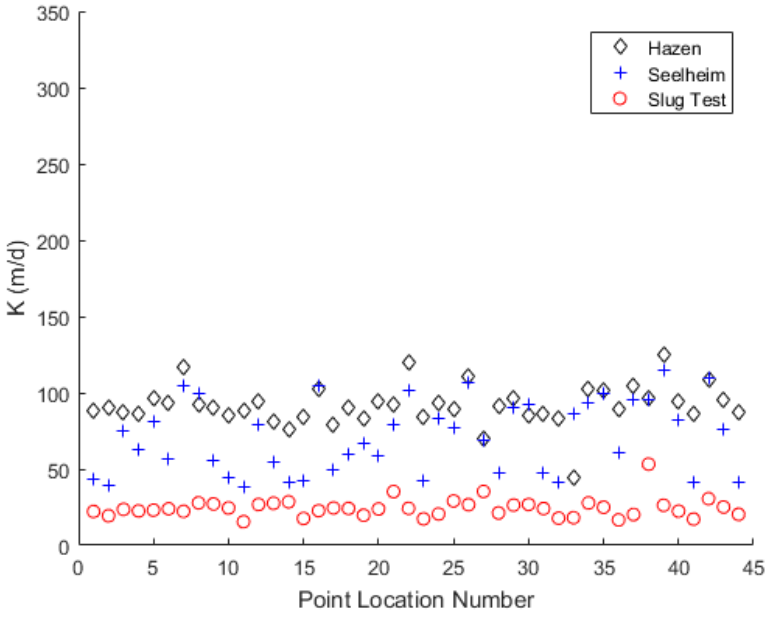

Figure 4-17: Scatter plot comparing empirical to slug test *K* from 6/02/2017.

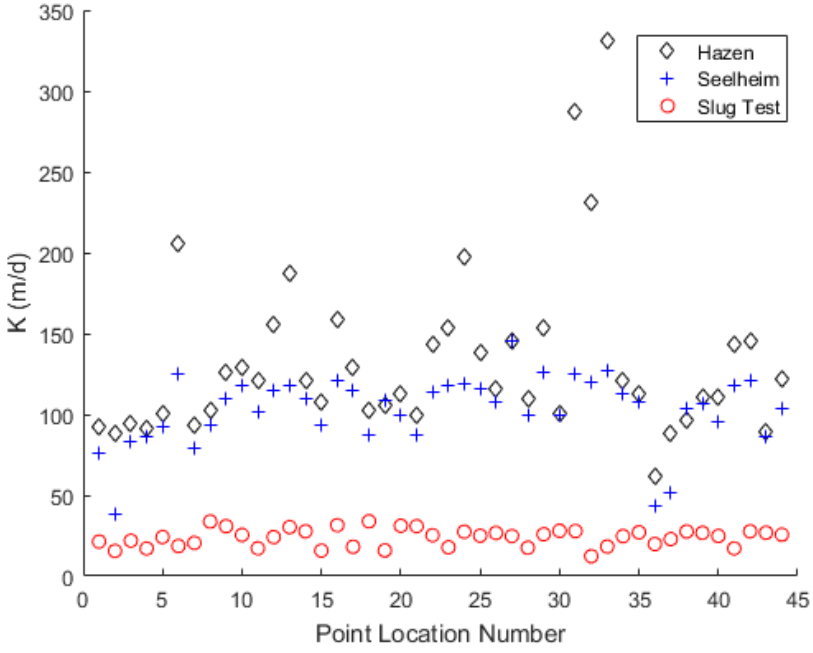

Figure 4-18: Scatter plot comparing empirical to slug test *K* from 7/05/2017.

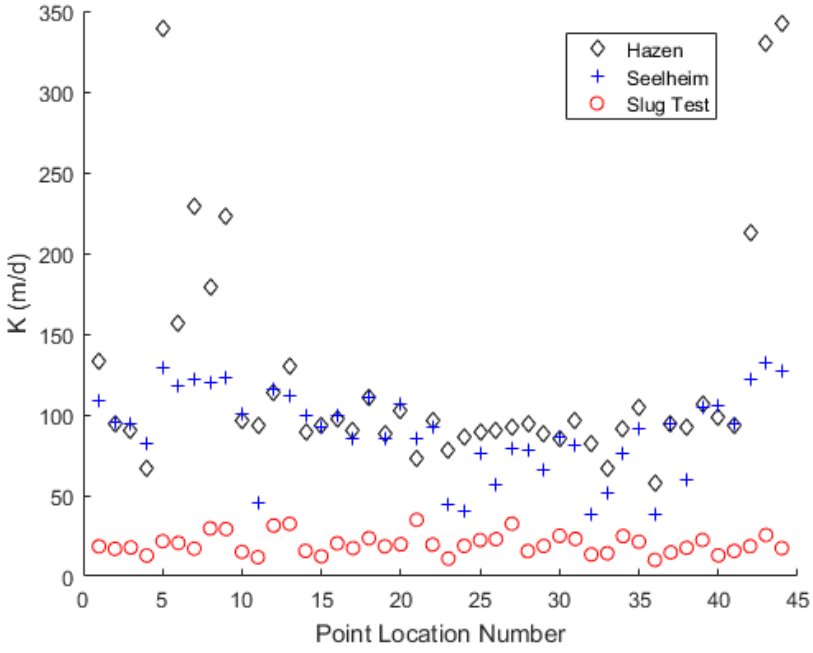

Figure 4-19: Scatter plot comparing empirical and slug test *K* from 8/03/2017.

Table 4-9 and figure 4-16 shows that 80-90% of the mass of each sample fell within 250 to 833 microns in diameter, meaning that all the processed samples were moderately well-sorted. On average, the sediments of the Loup River from the first, second, and third data collection events consisted of 97%, 97%, and 97.6% sand. Sediments also averaged 3%, 2.9%, and 2.3% gravel by weight from the three data collection events. Only samples from the third data collection event registered as having any silt or clay on average at 0.1%. Field observations suggest that the fine fraction of the Loup River's near surface sediments are composed of dominantly silt with very little clay, although no tests were done to quantify this observation. On average, it does not appear that the increase in discharge between the first and second collection events registered as a appreciable change in grain size in the stream.

K was empirically calculated from grain size using the Hazen and Seelheim methods for all 130 collected samples from each event. Figures 4-17 through 4-19, however, only compare values calculated from the 44 locations where both slug test and grain size data were collected. Of the plotted data, empirical *K* from the Hazen method was 276%, 454%, and 513% greater on average than slug test *K* for the first, second, and third data collection events, respectively. Of the plotted data, empirical *K* from the Seelheim method was 191%, 329%, and 354% greater on average than slug test *K* for the first, second, and third data collection events, respectively. Of the plotted data, the Hazen method produced *K* values that were 29%, 29%, and 35% greater on average than the Seelheim method from the first, second, and third data collections, respectively.

4.5 Statistical Analysis of *K* Data

4.5.1 Justification of Normal Distribution Assumption

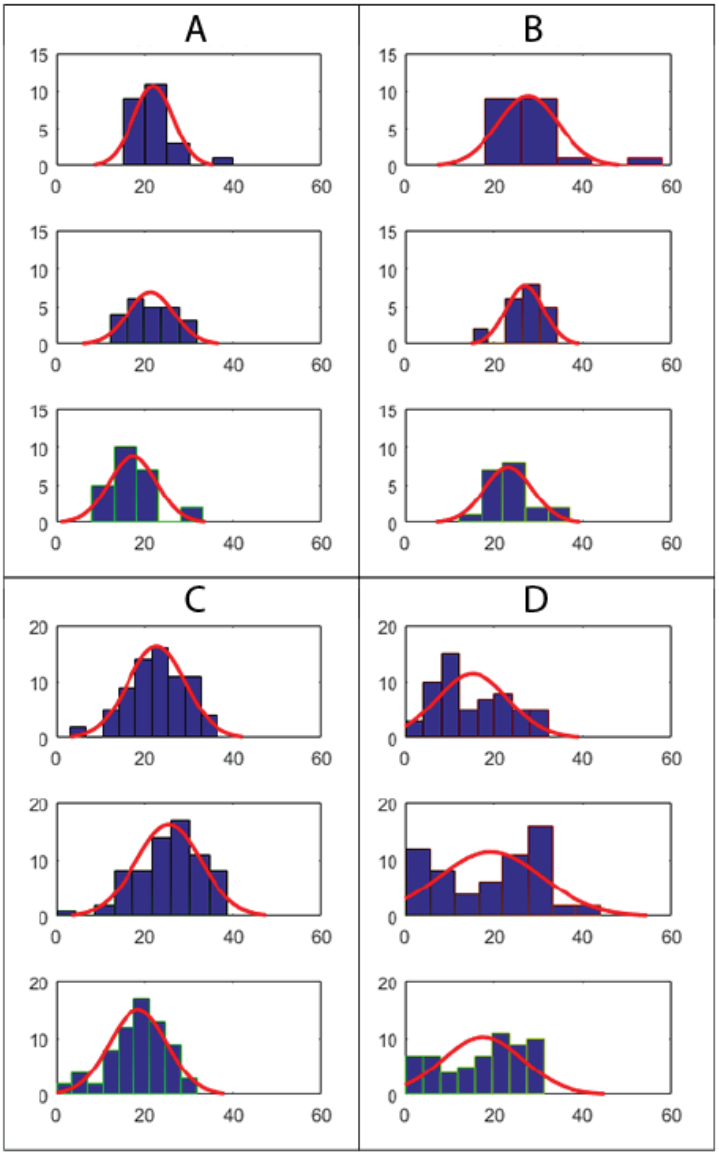

Figure 4-20: Histograms of permeameter (K_v) and slug test (K) with a normal distribution fit to the data. The x-axes represent K in meters/day and the y-axes represent the number of points that fell within a specified range of K values. Pane A is K data from immobile bar, B is K data from the mobile stream channel, C is K_v data from the immobile bar, D is K_v data from the mobile stream channel.

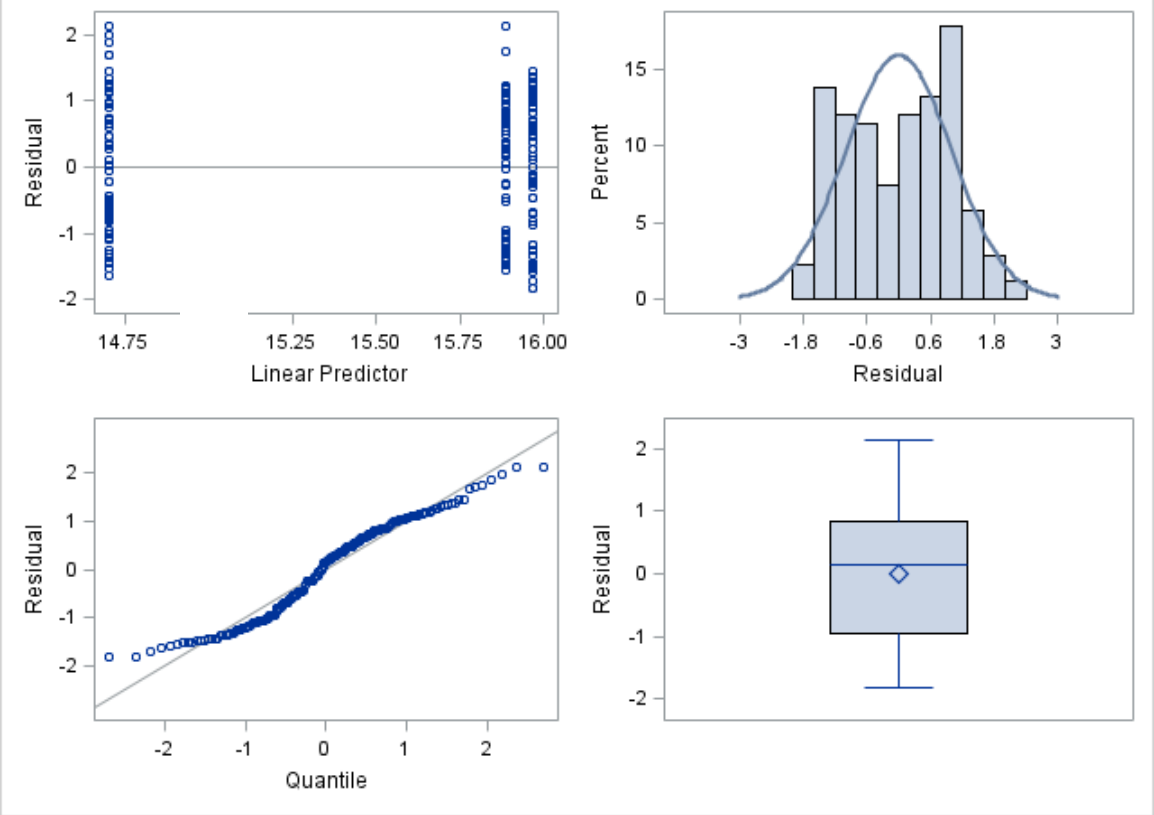

Figure 4-21: Residual plots used to visually test the assumption of a normal distribution and equal variances for K_v data from the immobile environment.

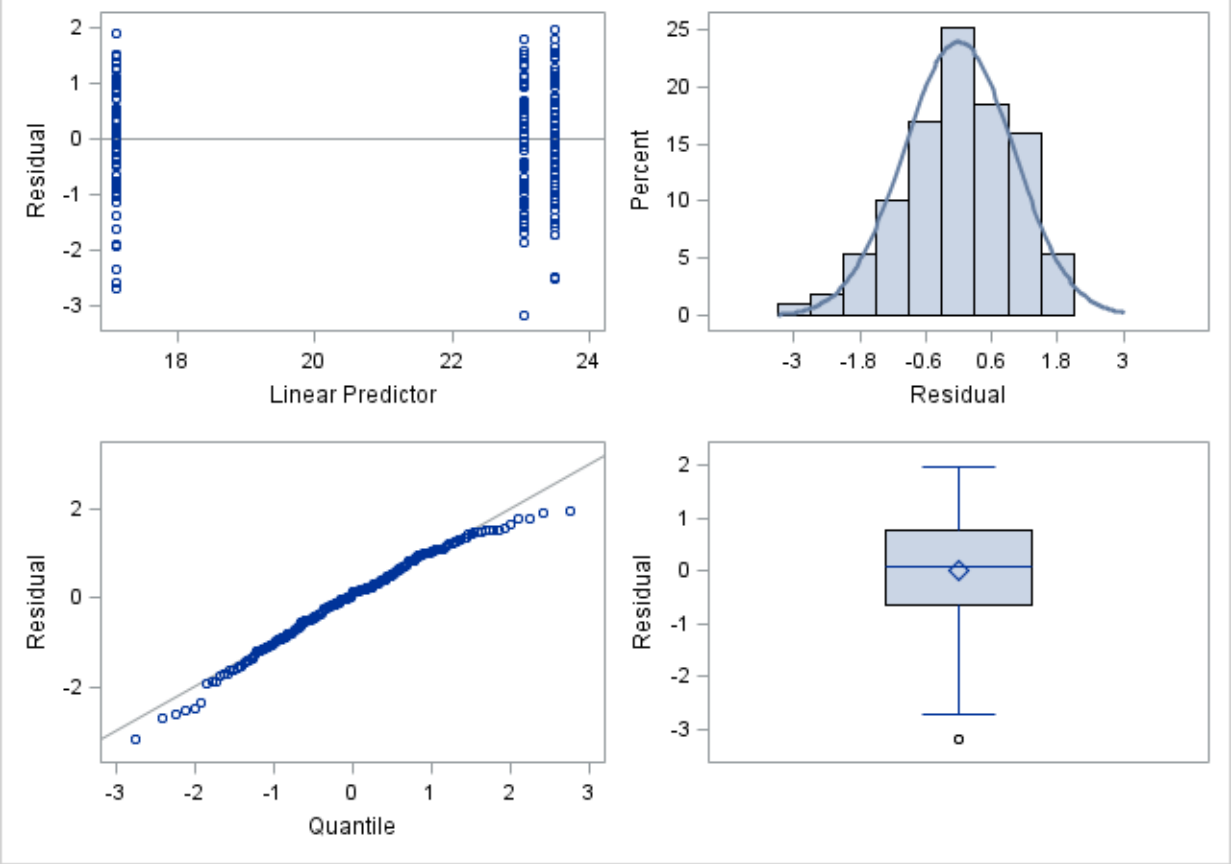

Figure 4-22: Residual plots used to visually test the assumption of a normal distribution and equal variances for K_v data from the mobile environment.

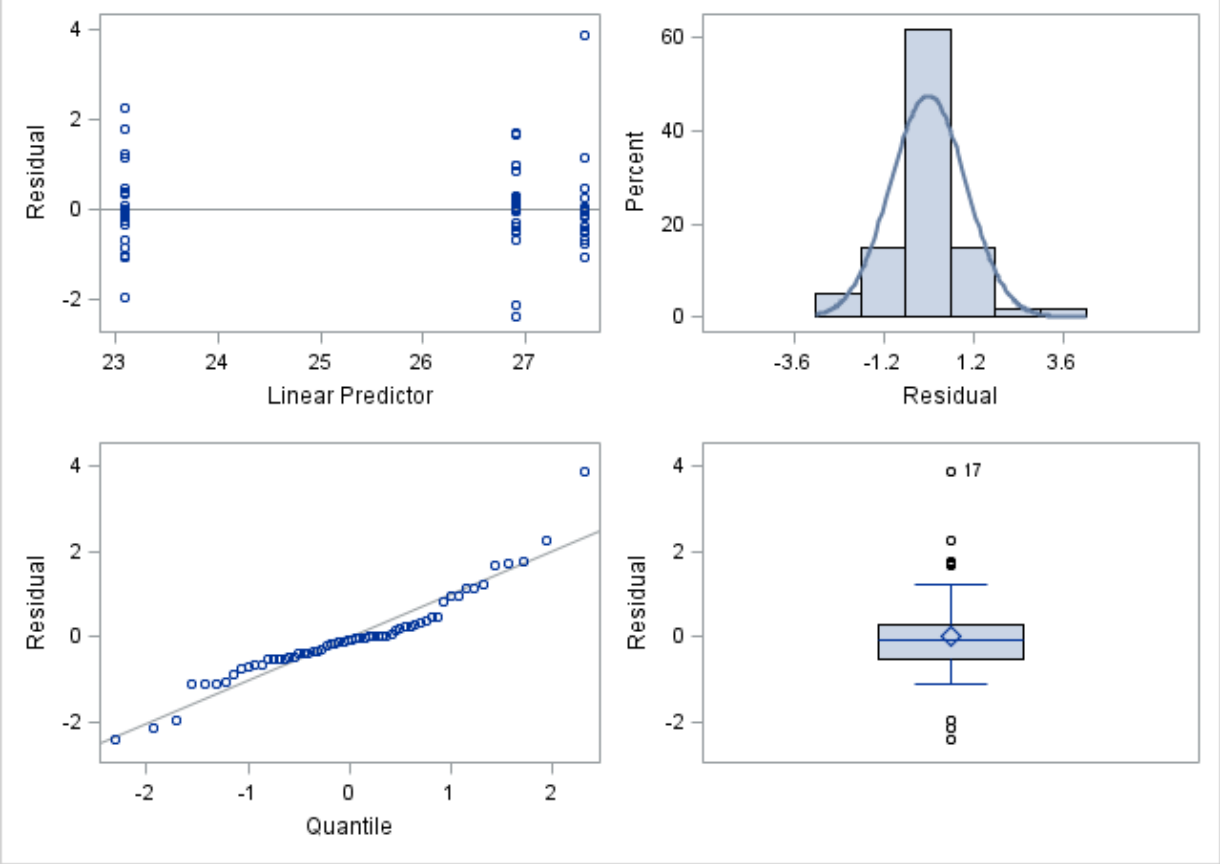

Figure 4-23: Residual plots used to visually test the assumption of a normal distribution and equal variances for *K* data from the immobile environment.

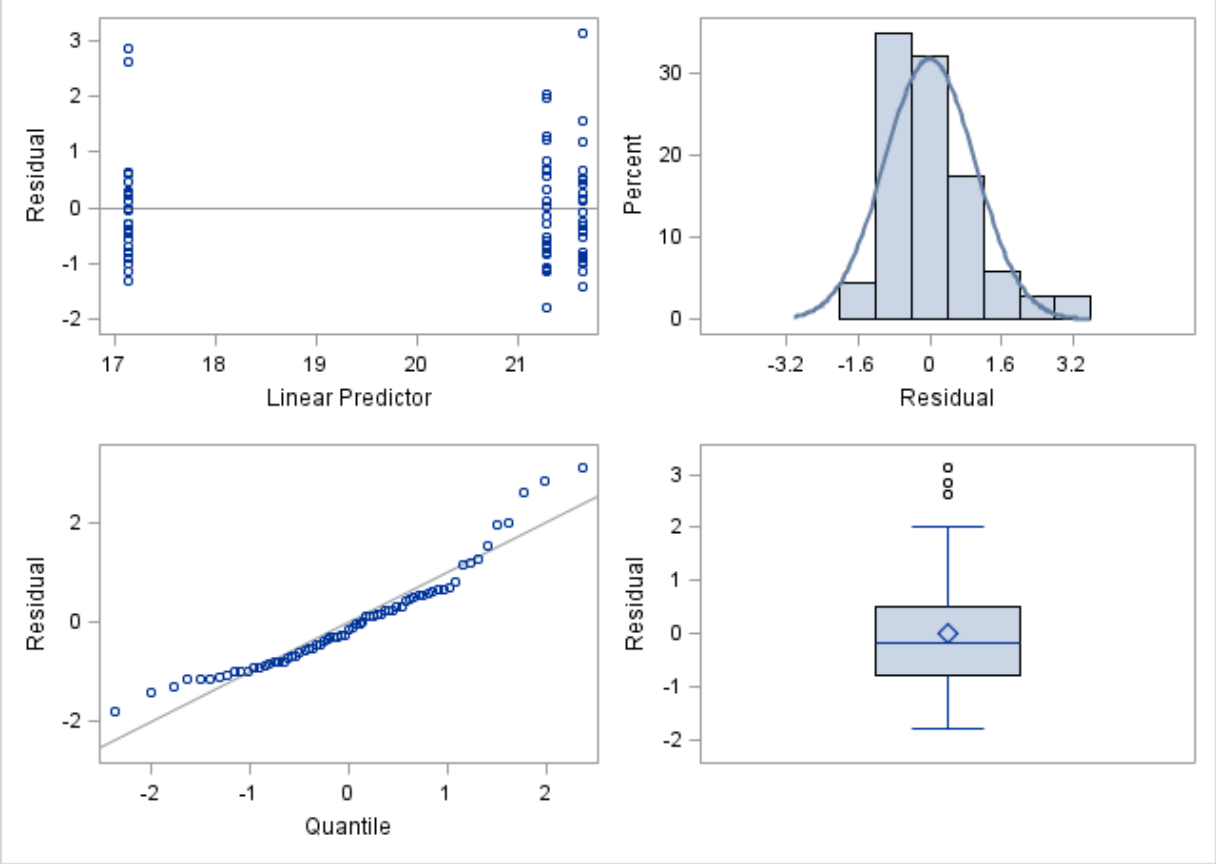

Figure 4-24: Residual plots used to visually test the assumption of a normal distribution and equal variances for *K* from the mobile environment.

Figure 4-20 demonstrates that the assumption of a normal distribution is reasonable for *K* and K_v data collected from each environment and each time. It should be noted that K_v data from the mobile stream channel has the worst fit to the normal distribution of all the data collected, and this distribution remains relatively poor throughout all three times when data was collected. Figures 4-21 through 4-24 also visually confirm the assumption of a normal distribution through residual and quantile plots, but these figures display data from all collection events categorized by environment and measurement type (*K* or K_v). Figures 4-21 through 4-24 also visually confirm the

assumption of equal variances via the residual plots in the upper left corner of each figure. The assumptions of a repeated measures ANOVA are that the data collected at different points in time are approximately normally distributed and have approximately equal variance.

4.5.2 Determination of Covariance Structure

Method	AICc
ANTE(1)	1216.99
AR(1)	1216.53
ARH(1)	***1215.13***
UN	1218.09
CS	1216.17

K_v Mobile

Method	AICc
ANTE(1)	1318.76
AR(1)	1326.37
ARH(1)	1330.07
UN	***1315.51***
CS	1326.05

K_v Immobile

Method	AICc
ANTE(1)	***359.03***
AR(1)	364.02
ARH(1)	361.40
UN	361.29
CS	367.16

K Mobile

Method	AICc
ANTE(1)	408.43
AR(1)	404.17
ARH(1)	406.87
UN	***392.77***
CS	394.89

K Immobile

Table 4-11: Results of AICc comparison of covariance structures to determine the model that best fits each dataset. The structures above are Ante Dependence: First Order {ANTE(1)}, First Order Autoregressive {AR(1)}, Heterogeneous Autoregressive {ARH(1)}, Unstructured {UN}, and Compound Symmetry {CS}. The model with the lowest AICC was used for the repeated measures analysis and is identified by bold and italicized text.

4.5.3 ANOVA Repeated Measures Analysis Results

Time	Average	Standard Error	Lower Confidence Interval	Upper Confidence Interval
6/02/2017	21.64	0.93	19.71	23.58
7/05/2017	21.27	1.08	19.04	23.51
8/03/2017	17.14	1.15	14.75	19.53

Table 4-12: Time least squares means of *K* data from the immobile environment.

Time 1	Time 2	Estimate	Standard Error	p-value	Lower Confidence Interval	Upper Confidence Interval
6/02/2017	7/05/2017	0.37	0.93	0.70	-1.56	2.29
6/02/2017	8/03/2017	4.50	0.71	<.0001	3.03	5.97
7/05/2017	8/03/2017	4.13	1.23	0.0029	1.58	6.69

Table 4-13: Differences of time least squares means for *K* from the immobile environment.

Time	Average	Standard Error	Lower Confidence Interval	Upper Confidence Interval
6/02/2017	27.57	1.53	24.48	30.66
7/05/2017	26.91	0.94	25.00	28.81
8/03/2017	23.10	1.21	20.65	25.56

Table 4-14: Time least squares means of *K* data from the mobile environment.

Time 1	Time 2	Estimate	Standard Error	p-value	Lower Confidence Interval	Upper Confidence Interval
6/02/2017	7/05/2017	0.67	1.60	0.68	-2.58	3.91
6/02/2017	8/03/2017	4.47	1.79	0.01	0.85	8.09
7/05/2017	8/03/2017	3.80	0.85	<.0001	2.08	5.52

Table 4-15: Differences of time least squares means for *K* from the mobile environment.

Time	Average	Standard Error	Lower Confidence Interval	Upper Confidence Interval
6/02/2017	23.50	0.83	21.83	25.16
7/05/2017	23.05	0.80	21.45	24.65
8/03/2017	17.11	0.70	15.70	18.51

Table 4-16: Time least squares means of K_v from the immobile environment.

Time 1	Time 2	Estimate	Standard Error	p-value	Lower Confidence Interval	Upper Confidence Interval
6/02/2017	7/05/2017	0.44	0.66	0.50	-0.88	1.77
6/02/2017	8/03/2017	6.39	0.89	<.0001	4.62	8.16
7/05/2017	8/03/2017	5.94	0.95	<.0001	4.05	7.83

Table 4-17: Differences of time least squares means for K_v from the immobile environment.

Time	Average	Standard Error	Lower Confidence Interval	Upper Confidence Interval
6/02/2017	14.70	1.02	12.68	16.72
7/05/2017	15.89	1.32	13.27	18.50
8/03/2017	15.97	1.10	13.78	18.15

Table 4-18: Time least squares means of K_v from the mobile environment.

Time 1	Time 2	Estimate	Standard Error	p-value	Lower Confidence Interval	Upper Confidence Interval
6/02/2017	7/05/2017	-1.18	1.22	0.33	-3.60	1.23
6/02/2017	8/03/2017	-1.26	1.32	0.34	-3.87	1.35
7/05/2017	8/03/2017	-0.08	1.25	0.95	-2.55	2.39

Table 4-19: Differences of time least squares means for K_v from the mobile environment.

T-grouping for time least squares means (α=0.05)											
Least squares means with the same letter are not significantly different.											
Immobile K_v			Mobile K_v			Immobile K			Mobile K		
Time	Estimate	Category	Time	Estimate	Category	Time	Estimate	Category	Time	Estimate	Category
6/02/2017	23.37	A	6/02/2017	16.46	C	6/02/2017	21.84	E	6/02/2017	27.51	G
7/05/2017	22.98	A	7/05/2017	16.06	C	7/05/2017	21.41	E	7/05/2017	26.73	G
8/03/2017	16.82	B	8/03/2017	14.91	C	8/03/2017	17.34	F	8/03/2017	22.77	H

Table 4-20: Summary of the repeated measures analyses results.

Table 4-11 shows that both K and K_v datasets from the mobile stream channel environment had inter-subject variability best described by an unstructured (UN) covariance model. Tables 4-12 through 4-19 provide interested readers with the detailed results of the repeated measures ANOVA. Note that the average values for each environment reported in this section are different than those reported in section 4.2 because point measurements where the location changed environment over the course of the study were excluded from the repeated measures analysis due to the variance they introduce. These points changed environment because the boundary between the immobile bar and mobile stream channel did not stay perfectly stable during the study period due to changes in stream stage. In these tables, p-values of less than 0.05 indicate that the null hypothesis of the repeated measures ANOVA can be reject at a 95% confidence interval. The null hypothesis of a repeated measures analysis is that the compared datasets do *not* have mean values that are statistically different from each other. P-values reported in these tables show that no significant statistical difference in means were found between the first and second data collection events from either environment or test (permeameter & slug). Statistical differences in means were found between the first and third, as well as the second and third data collection events for all environments and tests except mobile stream channel K_v, where no statistical difference in means was found between any of the three data collection events. Table 4-20 is a summary of the repeated measures analysis results presented in tables 4-12 through 4-19.

CHAPTER 5.0 DISCUSSION

5.1 Hypothesis Testing

This research tested the hypothesis that a time series of data on K and K_v would show greater statistical variability from the mobile stream channel relative to the immobile compound bar, because deposition and erosion are thought to be the primary controls on K transience in stream channel environments.

The results of the repeated measures analyses of the primary hydraulic data combined with the complimentary geophysical data strongly suggest that the proposed hypothesis of deposition and erosion as the dominant control on streambed K variability be rejected. The lack of statistically different means between mobile K_v datasets from any of the three collection events is direct evidence against the hypothesis. In addition, no statistically different means were found between mobile K or K_v datasets between 6/02/2017 and 7/05/2017. Statistically different means were found between mobile K datasets between 7/05/2017 and 8/03/2017, but statistically different means were also found between immobile K datasets between the same events. The fact that K was reduced across the entire study area between 7/05/2017 and 8/03/2017 makes interpreting the responsible processes difficult.

The interpretation of scour surfaces and channel incision from the GPR data (figures 4-13 and 4-15) is significant for the hypothesis because it confirms that the processes of deposition and erosion were occurring in the stream channel. The scour surfaces present in GPR profiles indicate that the effects of deposition and erosion were not limited to only the upper few centimeters of the streambed, but potentially affected depths as great as one meter below the sediment water interface. GPR also served as a

potential way to determine if deposition and erosion from the channel that cut into the compound bar portion of the grid affected a great enough depth to warrant changing the classification of the environment from immobile to mobile for the purpose of statistical analysis. Figures 4-12 and 4-15 illustrate the lack of change in sedimentary structure in the near subsurface of the bar relative to the stream channel. If reworking of the compound bar's subsurface did occur in response to this event, it did not penetrate through the entire zone investigated by the hydraulic tests. GPR data was not collected between 6/02/2017 and 7/05/2017, and changes in subsurface sedimentary structure are not known from that time. USGS stream gauge data, however, shows that between 6/02/2017 and 7/05/2017 discharge on the Loup River near Genoa varied between 1 and 10 m^3/day, which implies that deposition and erosion would have been occurring in the channel between those events.

As noted by Sebok (2015), K_v is especially sensitive to the presence of fine particle layers in the streambed. Field observations and K_v data (tables 4-6, 4-7, & figure 4-6) from 6/02/2017 and 7/05/2017 indicate that layers of silt were present in the stream channel. The extensive erosion and reworking of sediments captured by GPR in figure 4-15 between the second and third data collection events did not change K_v in the stream channel enough for the repeated measures analyses to reveal a significant difference between events.

The results of the repeated measures analyses do not support the alternative hypothesis that hyporheic remobilization of fine particles (diagenetic pore clogging) dominated K or K_v transience. The lack of statistically different means between K or K_v datasets from 6/02/2017 and 7/05/2017 suggest that pore clogging either wasn't active or

didn't change K or K_v significantly. Immobile K and K_v datasets from 7/05/2017 and 8/03/2017 do have statistically different means, and while K was significantly reduced across the entire study area, K_v was not. Grain size data shows that no appreciable increase in fine fraction sediments were recorded between 7/05/2017 and 8/03/2017 which would be expected from both pore clogging and deposition/erosion. This suggests that other processes such as bioclogging or gas ebullition may be responsible for the reduction of K and K_v.

5.2 Complications and Limitations

The interpretations above are complicated by the large anthropogenic increase in discharge that occurred on the Loup after cessation of water diversion from the LPPD's upstream canal. The observation that a small, cross bar channel was incised into the immobile compound bar between 7/05/2017 and 8/03/2017 is important because the hypothesis of this thesis is dependent upon comparing K changes in immobile sediments to those in mobile sediments. GPR profiles were used to address the degree to which the cross bar channel may have mobilized sediment within the upper 0.5 m of the saturated zone. The same interpreted sedimentary structures can be identified in GPR profiles collected before and after the flow event that formed the small channel, showing that the compound bar remained immobile overall (figure 4-12). At shallow depths (~ upper 10 – 15 cm), however, where GPR imagery is obfuscated by ground and air waves, it is difficult to determine whether sediments beneath the channel were mobilized. The varying stage heights between data collection events could also affect the hydraulic tests. However, field observations suggest that changes in stage during the study period would have been significantly less than the 30.48 cm screen length of slug test piezometers, or

the 50 cm of sediment tested with permeameters. This means that there would have been considerable overlap of the depth intervals tested for K and K_v from all three data collection events.

One potential weakness of this temporal K data is that the tubes and wells used to conduct measurements of K were removed and re-inserted at a slightly different location later, disturbing the sediment and potentially introducing measurement error into the data. Figure 4-6 and tables 4-6 and 4-7 show that the spatial pattern in K_v did not change appreciably between 6/02/2017 and 7/05/2017. This data shows that even though the exact location of each K measurement varied within one meter, this testing procedure could record the same general spatial pattern across the whole grid. It would be necessary to conduct a study dedicated to determining if re-installation has a significant effect on repeated K measurements, but it is believed to be negligible. The obvious solution to this problem would be to install semi-permanent tubes and wells into the streambed. However, this approach has its own weaknesses because in the stream channel the localized flow field around the installed tube or well would be modified with unknown effects on K over time. This method would also be more expensive, especially regarding purchasing enough wells to conduct slug tests at the density sampled in this study.

The fact that K was sampled in a less spatially dense pattern needs to be considered when comparing spatial patterns of K and K_v data. The number of points per area of streambed for K_v is approximately 0.14 points/m^2, while for K the value is approximately 0.05 points/m^2. It can be assumed that the spatial interpolations in figure 4-6 for K_v are accurate characterizations, while the interpolations of K in figure 4-5 can at

best be considered to reflect the correct average value of *K* over each environment (Kennedy et al. 2008).

5.3 Research Significance

This research is unique relative to other studies done on the temporal and spatial variability of streambed *K* because of its focus on change over time as a lens for understanding processes, and that it utilizes methods from hydrogeology, sedimentology, and geophysics. The employment of time-series GPR data within the streambed provides a novel illustration of streambed processes that is absent from other research on streambed *K* transience. The results of this study are consistent with work done by Genereux et al. (2008), Sebok et al. (2012), and others in showing that streambed *K* is temporally dynamic. The results however, suggest that deposition and erosion do not play as significant of a role in controlling changes in streambed *K* over seasonal timescales as some researchers have hypothesized.

The fact that streambed *K* is not static over time has implications for the study of groundwater-surface water interactions, groundwater modeling, as well as limnology and hyporheic exchange. When streams are included in groundwater models using software such as MODFLOW, streambed conductance is typically assumed to be a constant value in both time and space. The results of this study suggest that modeling groundwater-surface water interactions in this way is inaccurate, at least on short seasonal time scales. The need to incorporate realistic heterogeneity and temporal variability of streambed *K* can legitimately be questioned. Studies on the temporal variability of *K* over one year from West Bear Creek, NC by Genereux et al. (2008) suggests that streambed *K* may not vary enough over longer time periods to warrant attention in regional groundwater

models. *K* variability would be of greater significance for very localized models of groundwater-surface water interactions, especially those that attempt to model solute exchange between streams and alluvial aquifers.

The results of this study suggest that large increases in stream discharge, such as natural floods or anthropogenic events, may sometimes have a dampening effect that reduces *K* in sandy streambeds. This study recorded the changes in streambed *K* heterogeneity after a single high flow event, as well as the antecedent conditions. The findings are consistent with the work of Genereux et al. (2008) from West Bear Creek, NC where *K* measurements were made over one year and recorded both increases and decreases in *K* in response to high flow events. In this study, the recorded high flow event was anthropogenic and was characterized by a rapid increase in discharge followed by a minor subsequent drop and then sustained flow significantly greater than pre-event conditions. The anthropogenic nature of this event may be new to the study of streambed *K* transience.

Deposition and erosion have been hypothesized as the dominant controls on streambed *K* transience by several researchers (Genereux et al. 2008; Jiang et al. 2015; Sebok et al. 2015; Korus et al. 2017). This study reports that the constant deposition and erosion caused by variable flow velocity in active stream channels doesn't necessarily equate to greater *K* transience compared to inactive bars within the stream. The results of this study also do not support the conclusion that hyporheic pore clogging is more, or less, dominant than deposition and erosion over short periods of time. Large increases in flow that scour volumes of sediment from the streambed may not change *K* heterogeneity significantly. This is counter the logic of researchers such as Genereux et al. (2008), who

assumed that deposition and erosion were the dominant cause of changes in *K* observed after high flow events, but does not necessarily suggest that such an assumption is incorrect for different streams or events.

Diagenetic pore clogging did not produce a statistically significant change in either *K* or K_v on the compound bar between the first or second data collection events. This could indicate that the diagenetic processes do not act on time scales that would have allowed its effects to be recorded at the sampling frequency of this study, or it may indicate that these processes were not active at all during this time span. Other than measuring *K* directly and assuming the changes measured are due to pore clogging, the mechanism is difficult to measure and quantify.

The dampening of *K* and K_v observed from the compound bar between 7/05/2017 and 8/03/2017 suggests that one or more processes affecting K were active within the immobile sediments during that period. The specific process cannot be identified with certainty, as the effects of bar-top erosion and deposition, biological activity, and pore clogging were not specifically quantified in this research. The drop in electrical conductivity between 6/29/2017 and 8/09/2017 shown in figure 4-7, however, does provide evidence of a general decrease in porosity of the compound bar sediments due to the action of pore clogging. In sand deposits with little to no clay content, a direct relationship between *K* and electrical conductivity with porosity has been observed (Heigold et al. 1979). The observed decrease in electrical conductivity could be due to a decrease in porosity from one or more processes, such as the emplacement of fines or the build-up of biological material or gases in the pores. In figure 4-1, a progressive darkening of the exposed sands can be observed over time, as well as the development of

patches of green grass by August 1st. The influence of biological activity on *K* heterogeneity is otherwise difficult to quantify through field observations or otherwise.

Gases are released into streambed sediments from decay of organic materials and denitrification (Cuthbert et al. 2010; Dong et al. 2012). In the collected GPR profiles numerous hyperbolas can be observed such as those in figure 4-9. Field observations suggest that many of these hyperbolas represent the trunks or branches of trees deposited during high flow events. The likely existence of such buried organic material indicates a potential source of gas within the study area that could influence *K* transience. The land use of the area surrounding the field site is dominantly agricultural, and work by Dong et al. (2012) notes that denitrification does occur in Nebraska streams. Although no "sand rings" or gas bubbles emerging from the streambed were noticed, it is assumed that gas was present in the streambed from decay and denitrification.

The unquantified role of bioclogging and streambed gases introduces doubt to the assertion that the high flow event near the end of the study was responsible for the changes in *K* heterogeneity seen on 8/03/2017. Hypothetically, large increases in the prevalence of bioclogging, gas generation, or both between 7/05/2017 and 8/03/2017 could have caused the observed decline in *K* and K_v without the need for a high flow event. It is also possible that the anthropogenic high flow event could have been the stimulus for bioclogging or gas ebullition. The high flow event could have brought in nutrients to the study area that increased the growth rate of interstitial bacteria and subsequent bioclogging.

K_v mean and maximum values were only 1.3% and 17.5% smaller than *K* values. This relative closeness is surprising because it is generally assumed that streambed

sediments are significantly anisotropic, with horizontal K being much greater than K_v. It is important to recognize that slug test K is not exactly horizontal K because of the three-dimensional nature of the flow field that surrounds well screens. If the slug test K value is assumed to represent *primarily* horizontal K, then this data suggests that shallow sandy streambed sediments have relatively low anisotropy. Apparent anisotropy was observed in parts of the study grid, as evidenced by the fact that minimum K_v values were 54% smaller than minimum K values. This anisotropy tends to occur where a thin layer of mud is present on the streambed.

Tables 4-2 through 4-4 show that, in contrast to the K_v data, K was generally higher in the stream channel than on the compound bar. Field observations do not as readily explain this phenomenon as they did for K_v. More research comparing compound bar and stream channel K and K_v are needed to confirm if these observations can be generalized and assumed to be present in all sandy streambeds.

Extrapolations made from this research to other streams must take the grain size data into consideration. It would be best to limit such extrapolations to only streambeds with sediments comprised overwhelmingly of sand, with some gravel, and a very miniscule amount of silt and clay. Korus et al. (2017) noted that although silt constituted an extremely small fraction of the total sediment volume in the Loup River, it had a dominant effect on K_v heterogeneity. This underscores the need to only make extrapolations to streams with similar grain size distributions.

The poor correlation of both empirical methods of deriving K with slug test results could be due to the unconsolidated nature of sediments in the upper half meter of the streambed. This explanation is inconsistent with the findings of Cardenas & Zlotnik

(2003a), where empirically derived *K* was observed to have a strong correlation with slug and constant head tests from the Prairie Creek streambed in Nebraska. The fact that streambed *K* data from this study reasonably match a normal distribution is consistent with findings by Cardenas & Zlotnik (2003a) from Nebraska, but inconsistent with the findings of Genereux et al. (2008) from North Carolina.

CHAPTER 6.0 RECOMMENDATIONS FOR FUTURE WORK

There is a need for a study that refines the methods used in this research to elucidate the error introduced into repeated measures of *K* when instruments (tubes & wells) are removed and subsequently re-installed in the streambed in close proximity to the original measurement. Specifically, this method should be compared to measurements made using instruments that are installed in the streambed but not removed. Such a study is difficult to design in actual streambeds, because each method cannot be tested in the same location, and significant *K* heterogeneity exists within streambeds. It's conceivable that such a study could be performed in an artificial streambed environment, where sediment particles size is known explicitly and *K* does not change spatially or temporally.

The data presented here should only be extrapolated to streambeds transporting sediments with similar grain size distributions to those reported here. This presents research opportunities for similar studies on streams with sediments that differ in grain size and sorting. Specifically, data from a clay and silt dominated system would make a very interesting comparison. Although collecting data on *K* from such environments would be time consuming and present several logistical challenges.

This study explored changes in *K* heterogeneity strictly at a half meter below the sediment-water interface. A similarly structured study that examines three-dimensional changes in *K* over time would significantly add to the understanding of streambed processes. A potential hypothesis could be that *K* heterogeneity near the sediment water interface (within a meter) would be more variable than *K* heterogeneity at greater depths. Collecting this type of data would be even more physically demanding and logistically challenging than the work conducted in the present study.

The results of this study suggest that the response of streambed *K* heterogeneity to high flow events is worth investigating. Such work would be challenging due to the unpredictability of natural high flow events, but if anthropogenic releases from hydroelectric facilities were accepted as an analog the obstacle of unpredictability could be overcome. The work of Genereux suggests that average K_v can both increase and decrease in response to high flow events. Changes in *K* could potentially be recorded in response to varying magnitudes of high flow events, as well varying habits such as the rate of return to antecedent flow.

There exists a potential for research investigating the influence of biological activity and gas ebullition on streambed *K* heterogeneity. These processes are inherently difficult to quantify and separate from other active processes, and as such there is a need for engineering advances as well as method refinement studies. It is possible that, at least during biologically active seasons of the year, biofilms and gases could play a significant role in controlling streambed *K* transience.

This research suggests that GPR can be a useful tool for imaging streambed sedimentary architecture as well as hydrogeological and geomorphological research. With the proper application of processing steps, noisy GPR data collected through the water column can be transformed into useful profiles. Most GPR studies in fluvial environments have focused on exposed bar and bank sediments. A method refinement study that compares different center frequency antennas and processing techniques would be useful for data collected through the water column.

CHAPTER 7.0 CONCLUSIONS

This research used a time series of data on streambed *K* heterogeneity to understand the processes that control temporal variability of *K*. Bouwer and Rice slug testing (*K*) and permeameters (K_v) were used to directly measure streambed *K* at half a meter below the sediment water interface on 6/02/2017, 7/05/2017, and 8/03/2017. Complimentary geophysical surveys and grain size analyses were also conducted to record changes in sedimentary structure.

This study has demonstrated that streambed *K* is a spatially and temporally variable property on time scales as short as three months. *K* data collected through slug testing was observed to decrease 2% between 6/02/2017 and 7/05/2017, and decreased by 17% between 7/05/2017 and 8/03/2017. The latter of these was determined to be statistically significant for both the immobile and mobile environments using repeated measures analyses. K_v data collected from falling head permeameters was observed to increase 16.5% between 6/02/2017 and 7/05/2017, and decrease 20% between 7/05/2017 and 8/03/2017. K_v data from the final dataset was determined to be statistically different from the other two collection events from only the immobile bar environment using repeated measures analyses.

Despite GPR data that recorded deposition and erosion actively reworking the mobile stream channel, repeated measures analyses did not demonstrate a statistically significant change in K_v in the stream channel between any data collection events. This evidence, in conjunction with a lack of statistical difference in *K* or K_v between the first and second sampling events from either streambed environment, requires the hypothesis that deposition and erosion dominate the variability of streambed *K* be rejected. The

results of this research suggest that bioclogging and gas ebullition processes need to be further studied as causes of streambed *K* variability. It also suggests that anthropogenic high flow events can trigger changes in streambed *K* heterogeneity from antecedent conditions, although the specific causes of *K* reduction have yet to be elucidated.

This research demonstrates the efficacy of utilizing a combination of hydrogeological, geophysical, and sedimentological methods to capture short-term temporal changes in streambed *K* heterogeneity and the factors that influence it. Specifically, time series GPR data can capture changes in sedimentary architecture caused by erosion and subsequent deposition of sediment in an actively flowing channel. In this streambed, empirically derived *K* from grain size data did not have a strong correlation with *K* derived through slug testing. Extrapolations from this research about the processes occurring in other streambeds should be limited to only those composed overwhelmingly of sand, with some gravel, and miniscule amounts of silt and clay.

REFERENCES

Bjerg, P., K. Hinsby, T. Christensen, and P. Gravesen. 1992. Spatial Variability of Hydraulic Conductivity of an Unconfined Sandy Aquifer Determined by a Mini Slug Test. *Journal of Hydrology* 136 (1–4): 107–22. doi:10.1016/0022-1694(92)90007-I.

Blott, S., and K. Pye. 2001. Gradistat: A Grain Size Distribution and Statistics Package for the Analysis of Unconcolidated Sediments. *Earth Surface Processes and Landforms* 26: 1237–1248. doi:10.1002/esp.261.

Boulton, A., S. Findlay, P. Marmonier, E. Stanley, and H Valett. 1998. The Functional Significance of the Hyporheic Zone in Streams and Rivers. *Annual Review of …* 29 (1998): 59–81. doi:10.1146/annurev.ecolsys.29.1.59.

Bouwer, H., and R. Rice. 1976. A Slug Test for Determining Hydraulic Conductivity of Unconfined Aquifers with Completely or Partially Penetrating Wells. *Water Resources Research* 12 (3): 423–28. doi:10.1029/WR012i003p00423.

Burrell, J., H. Gurrola, and K. Mickus. 2008. Frequency Domain Electromagnetic and Ground Penetrating Radar Investigation of Ephemeral Streams: Case Study near the Southern High Plains, Texas. *Environmental Geology* 55 (6): 1169–79. doi:10.1007/s00254-007-1063-5.

Cardenas, M., J. Wilson, and V. Zlotnik. 2004. Impact of Heterogeneity, Bed Forms, and Stream Curvature on Subchannel Hyporheic Exchange. *Water Resources Research* 40 (8): 1–14. doi:10.1029/2004WR003008.

Cardenas, M., and V. Zlotnik. 2003a. Three-Dimensional Model of Modern Channel Bend Deposits. *Water Resources Research* 39 (6): 1–13. doi:10.1029/2002WR001383.

———. 2003b. A Simple Constant-Head Injection Test for Streambed Hydraulic Conductivity Estimation. *Ground Water* 41 (6): 867–71. doi:10.1111/j.1745-6584.2003.tb02428.x.

Chen, X. 2000. Measurement of Streambed Hydraulic Conductivity and Its Anisotropy. *Environmental Geology* 39 (12): 1317–24. doi:10.1007/s002540000172.

———. 2004. Streambed Hydraulic Conductivity for Rivers in South-Central Nebraska. *Journal of the American Water Resources Association* 40 (3): 561–73. doi:10.1111/j.1752-1688.2004.tb04443.x.

Conant, B. 2004. Delineating and Quantifying Ground Water Discharge Zones Using Streambed Temperatures. *Ground Water* 42 (2): 243–57. doi:10.1111/j.1745-6584.2004.tb02671.x.

Cuthbert, M., R. Mackay, V. Durand, M. Aller, R. Greswell, and M. Rivett. 2010. Impacts of River Bed Gas on the Hydraulic and Thermal Dynamics of the Hyporheic Zone. *Advances in Water Resources* 33 (11): 1347–58. doi:10.1016/j.advwatres.2010.09.014.

Dey, S. 2014. Introduction. In *Fluvial Hydrodynamics: Hydrodynamic and Sediment Transport Phenomena*, 1–27. Berlin, Heidelberg: Springer Berlin Heidelberg. doi:10.1007/978-3-642-19062-9_1.

Diez, D. 2015 OpenIntro Statistics Third Edition. doi:Diez, D. M., & Barr, C. D. (2015). OpenIntro Statistics Second Edition.

Dingman, L. 1978. Drainage Density and Streamflow : A Closer Look. *Water Resources Research* 14 (6): 1183-1187.

Domenico, P., and F. Schwartz. 1990. *Physical and Chemical Hydrogeology*. Second. New York, NY: John Wiley & Sons.

Dong, W., X. Chen, Z. Wang, G. Ou, and C. Liu. 2012. Comparison of Vertical Hydraulic Conductivity in a Streambed-Point Bar System of a Gaining Stream. *Journal of Hydrology* 450–451. Elsevier B.V.: 9–16. doi:10.1016/j.jhydrol.2012.05.037.

Eaton, T. 2006. On the Importance of Geological Heterogeneity for Flow Simulation.

Sedimentary Geology 184 (3–4): 187–201. doi:10.1016/j.sedgeo.2005.11.002.

Ellyson, T. 2017. Waiver Allows Canal Diversion to Resume. *The Columbus Telegram*, July 17. http://columbustelegram.com/news/local/waiver-allows-canal-diversion-to-resume/article_22f3c2fc-4dc7-591e-a508-725208f0f47d.html.

Genereux, D., S. Leahy, H. Mitasova, C. Kennedy, and D. Corbett. 2008. Spatial and Temporal Variability of Streambed Hydraulic Conductivity in West Bear Creek, North Carolina, USA. *Journal of Hydrology* 358 (3–4): 332–53. doi:10.1016/j.jhydrol.2008.06.017.

Giraud, C. 2014. *Introduction to High-Dimensional Statistics*. Chapman & Hall/CRC Monographs on Statistics & Applied Probability. CRC Press. https://books.google.com/books?id=iUQqBgAAQBAJ.

Girden, E. 2017. Introduction. In *ANOVA: Repeated Measures*, 1–2. Thousand Oaks: SAGE Publications, 2011.

Hazen, A. 1893. Some Physical Properties of Sand and Gravels, with Special Reference to Their Use in Filtration. Twenty Fourth Annual Report, State Board of Health of Massachusetts 541-556.

Heberer, T., I. Verstraeten, M. Meyer, A. Mechlinski, and K. Reddersen. 2011. Occurrence and Fate of Pharmaceuticals during Bank Filtration–preliminary Results from Investigations in Germany and the United States. *Journal of Contemporary Water Research and Education* 120 (1): 2. http://opensiuc.lib.siu.edu/cgi/viewcontent.cgi?article=1153&context=jcwre.

Heigold, P., R. Gilkeson, K. Cartwright, and P. Reed. 1979. Aquifer Transmissivity from Surficial Electrical Methods. *Ground Water* 17 (4). Blackwell Publishing Ltd: 338–45. doi:10.1111/j.1745-6584.1979.tb03326.x.

High Plains Regional Climate Center. Regional Climate Center CLIMOD Page. Accessed

December 1st, 2017. https://hprcc.unl.edu/.

Hu, S. 1987. Akaike Information Criterion Statistics. *Mathematics and Computers in Simulation* 29 (5): 452. doi:10.1016/0378-4754(87)90094-2.

Huggenberger, P., and T. Aigner. 1999. Introduction to the Special Issue on Aquifer-Sedimentology: Problems, Perspectives and Modern Approaches. *Sedimentary Geology* 129 (3–4): 179–86. doi:10.1016/S0037-0738(99)00101-3.

Hvorslev M. 1951. Time Lag and Soil Permeability in Groundwater Observations. *Waterways Experiment Station US Arym Corps of Engineers,* Vicksburg, MI

Jiang, W., J. Song, J. Zhang, Y. Wang, N. Zhang, X. Zhang, Y. Long, J. Li, and X. Yang. 2015. Spatial Variability of Streambed Vertical Hydraulic Conductivity and Its Relation to Distinctive Stream Morphologies in the Beiluo River, Shaanxi Province, China. *Hydrogeology Journal*, no. 2010: 1617–26. doi:10.1007/s10040-015-1288-4.

Annan, A. Electromagnetic Principles of Ground Penetrating Radar. In *Ground Penetrating Radar: Theory and Applications,* edited by H. Jol, 3-38. Amsterdam: Elsevier Science, 2009.

Kennedy, D., D. Genereux, H. Mitasova, D. Corbett, and S. Leahy. 2008. Effect of Sampling Density and Design on Estimation of Streambed Attributes. *Journal of Hydrology* 355 (1–4): 164–80. doi:10.1016/j.jhydrol.2008.03.018.

Kirsch, R. Electromagnetic Methods - Frequency Domain. In *Groundwater Geophysics: A Tool for Hydrogeology*. *Environmental and Engineering Geoscience*, edited by R. Kirsch, 155-176. Vol. 17. Berlin: Springer, 2006.

Koltermann, C., and S. Gorelick. 1996. Heterogeneity in Sedimentary Deposits: A Review of Structure-Imitating, Process-Imitating, and Descriptive Approaches. *Water Resources*

Research 32 (9): 2617–58. doi:10.1029/96WR00025.

Korus, J., T. Gilmore, M. Waszgis, and A. Mittelstet. 2017. Unit-Bar Migration and Bar-Trough Deposition: Impacts on Hydraulic Conductivity and Grain Size Heterogeneity in a Sandy Streambed. *Hydrogeology Journal*, September. doi:10.1007/s10040-017-1661-6.

Landon, M., D. Rus, and F. Harvey. 2001. Comparison of Instream Methods for Measuring Hydraulic Conductivity in Sandy Streambeds. *Groundwater* 39 (6): 870–85. doi:10.1111/j.1745-6584.2001.tb02475.x.

Lee, D., and J. Cherry. 1979. A Field Exercise on Groundwater Flow Using Seepage Meter and Mini-Piezometers. *Journal of Geological Education* 27: 6–9.

Levy, J., Birck, M., Mutiti, S., Kilroy, K., Windeler, B., Idris, O., Allen, L. 2010. The Impact of Storm Events on a Riverbed System and its Hydrualic Conductivity at a Site of Induced Infiltration. *Journal of Environmental Management* (92): 1960-1971. doi: 10.1016/j.jenvman.2011.03.017

Lipka, A., and B. Tyner. Repeated Measures Covariance Structure. Accessed December 20th, 2017. http://www.stat.purdue.edu/~bacraig/SCS/rmcs.pdf.

Lund Research. Repeated Measures ANOVA. Accessed December 20th, 2017. https://statistics.laerd.com/statistical-guides/repeated-measures-anova-statistical-guide.php.

Marsily, G., F. Delay, J. Gonçalvès, P. Renard, V. Teles, and S. Violette. 2005. "Dealing with Spatial Heterogeneity." *Hydrogeology Journal* 13 (1): 161–83. doi:10.1007/s10040-004-0432-3.

Morrice, J., H. Valett, C. Dahm, and M. Campana. 1997. Alluvial Characteristics, Groundwater–Surface Water Exchange and Hydrological Retention in Headwater Streams. *Hydrological Processes* 11 (3): 253–67. doi:10.1002/(SICI)1099-1085(19970315)11:3<253::AID-

HYP439>3.0.CO;2-J.

Mumpy, A., H. Jol, W. Kean, and J. Isbell. 2007. Architecture and Sedimentology of an Active Braid Bar in the Wisconsin River Based on 3-D Ground Penetrating Radar. In *Special Paper 432: Stratigraphic Analyses Using GPR*, 111–31. Geological Society of America. doi:10.1130/2007.2432(09).

Newcomer, M., S. Hubbard, J. Fleckenstein, U. Maier, C. Schmidt, M. Thullner, C. Ulrich, N. Flipo, and Y. Rubin. 2016. Simulating Bioclogging Effects on Dynamic Riverbed Permeability and Infiltration. *Water Resources Research* 52 (4): 2883–2900. doi:10.1002/2015WR018351.

Nicholas, P., P. Ashworth, M. Kirkby, M. Macklin, and T. Murray. 1995. Sediment Slugs: Large-Scale Fluctuations in Fluvial Sediment Transport Rates and Storage Volumes. *Progress in Physical Geography* 19 (4): 500–519. doi:10.1177/030913339501900404.

Nowinski, J., M. Cardenas, and A. Lightbody. 2011. Evolution of Hydraulic Conductivity in the Floodplain of a Meandering River due to Hyporheic Transport of Fine Materials. *Geophysical Research Letters* 38 (1): n/a-n/a. doi:10.1029/2010GL045819.

Pérez-Paricio, A., J. Hunink, E. Kupper, J. Quintana, and J Raso. 2010. Estimation of the River Conductance Coefficient Using Streambed Slope for Modeling of Regional River-Aquifer Interaction. *18th International Conference on Water Resources*, 9.

Leopold, L., and W. Bull. 1979. Base Level, Aggredation, and Grade. *American Philosophical Society* 123 (3): 168-202.

Annan, A. GPR Methods for Hydrogeological Studies. In *Hydrogeophysics*, Edited by Y. Rubin and S. Hubbard, 185-215. Dordrectcht: Springer, 2005.

Sebok, E., C. Duque, P. Engesgaard, and E. Boegh. 2015. Spatial Variability in Streambed

Hydraulic Conductivity of Contrasting Stream Morphologies: Channel Bend and Straight Channel. *Hydrological Processes* 29 (3): 458–72. doi:10.1002/hyp.10170.

Seelheim, F. 1880. Methoden Zur Bestimmung Der Durchlässigkeit Des Bodens. *Zeitschrift Für Analytische Chemie* 19 (1): 387–418. doi:https://doi.org/10.1007/BF01341054.

Smith, N. 1974. Sedimentology and Bar Formation in the Upper Kicking Horse River, a Braided Outwash Stream. *The Journal of Geology* 82 (2): 205–23. doi:10.1086/627959.

Sniegocki, R., and R. Langford. 1959. "Geologic and Ground-Water Reconnaissance of the Loup River Drainage Basin, Nebraska, with a Section on Chemical Quality of the Water." *Water Supply Paper*. http://pubs.er.usgs.gov/publication/wsp1493.

Springer, A., W. Petroutson, and B. Semmens. 1999. Spatial and Temporal Variability of Hydraulic Conductivity in Active Reattachment Bars of the Colorado River, Grand Canyon. *Ground Water* 37 (3): 338–44. doi:10.1111/j.1745-6584.1999.tb01109.x.

Syvitski, J., M. Morehead, D. Bahr, and T. Mulder. 2000. Estimating Fluvial Sediment Transport: The Rating Parameters. *Water Resources Research* 36 (9): 2747–60. doi:10.1029/2000WR900133.

Tzanis, A. 2006. Matgpr: A Freeware Matlab Package for the Analysis of Common-Offset GPR Data. *Geophysical Research Abstracts* 8. http://meetings.copernicus.org/www.cosis.net/abstracts/EGU06/09488/EGU06-J-09488.pdf.

USGS. National Hydrography Geodatabase: The National Map. Accessed November 17th, 2017. https://viewer.nationalmap.gov/viewer/nhd.html?p=nhd.

Valett, M., J. Morrice, C. Dahm, and M. Campana. 1996. Parent Lithology, Surface-Groundwater Exchange, and Nitrate Retention in Headwater Streams. *Limnology and Oceanography* 41 (2): 333–45. doi:10.4319/lo.1996.41.2.0333.

Zlotnik, V. 1994. Interpretation of Slug and Packer Tests in Anisotropic Aquifers. *Groundwater*. doi:10.1111/j.1745-6584.1994.tb00917.x.

Zlotnik, V., H. Huang, and J. Butler. 1999. Evaluation of Stream Depletion Considering Finite Stream Width, Shallow Penetration, and Properties of Streambed Sediments. In *Water 99: Joint Congress; 25th Hydrology & Water Resources Symposium, 2nd International Conference on Water Resources & Environment Research; Handbook and Proceedings*.

APPENDIX A: PLOTS OF REPRESENTATIVE SLUG TEST RECOVERY CURVES

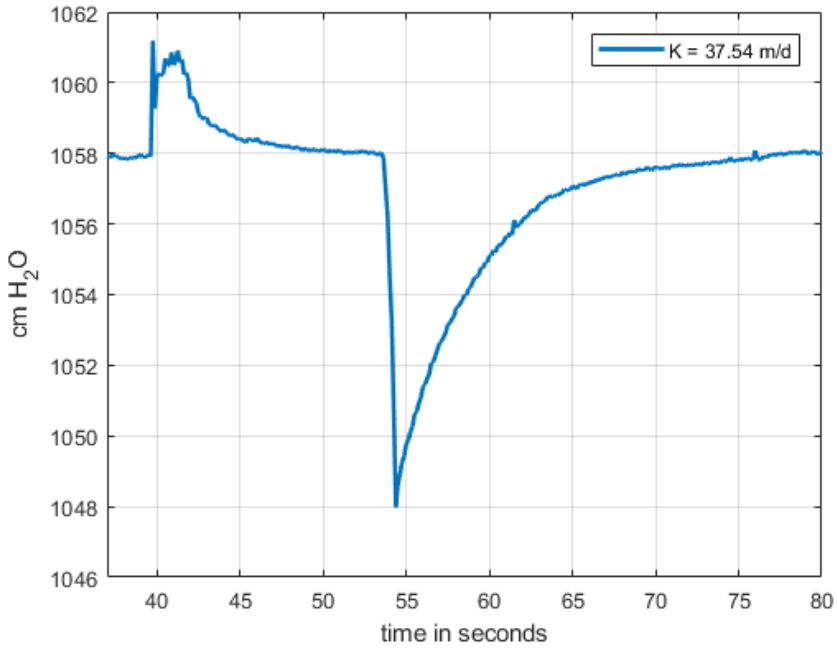

Figure A-1: Recovery curve from the first slug test conducted at point E9 from 6/02/2017.

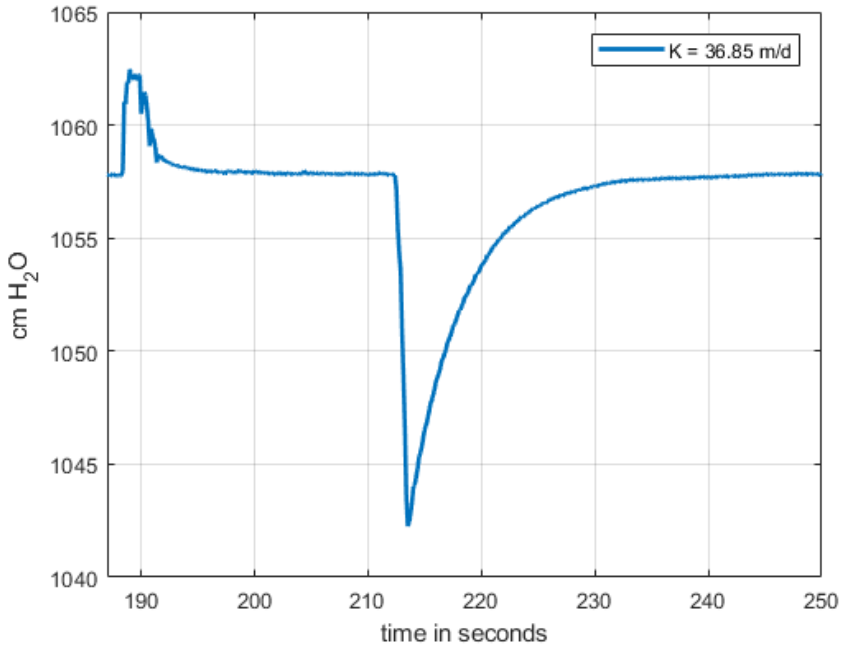

Figure A-2: Recovery curve from the second slug test conducted at point E9 from 6/02/2017.

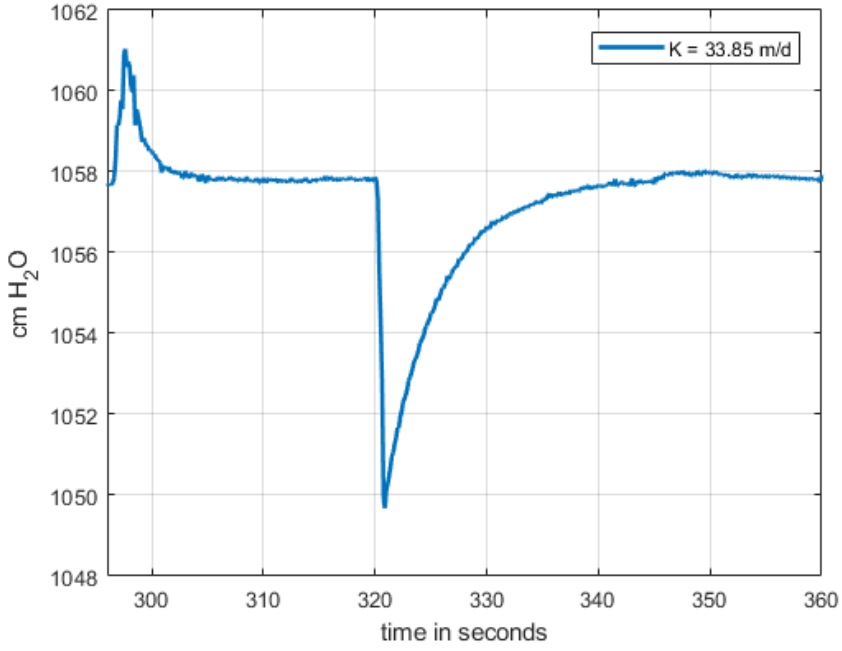

Figure A-3: Recovery curve from the third slug test conducted at point E9 from 6/02/2017.

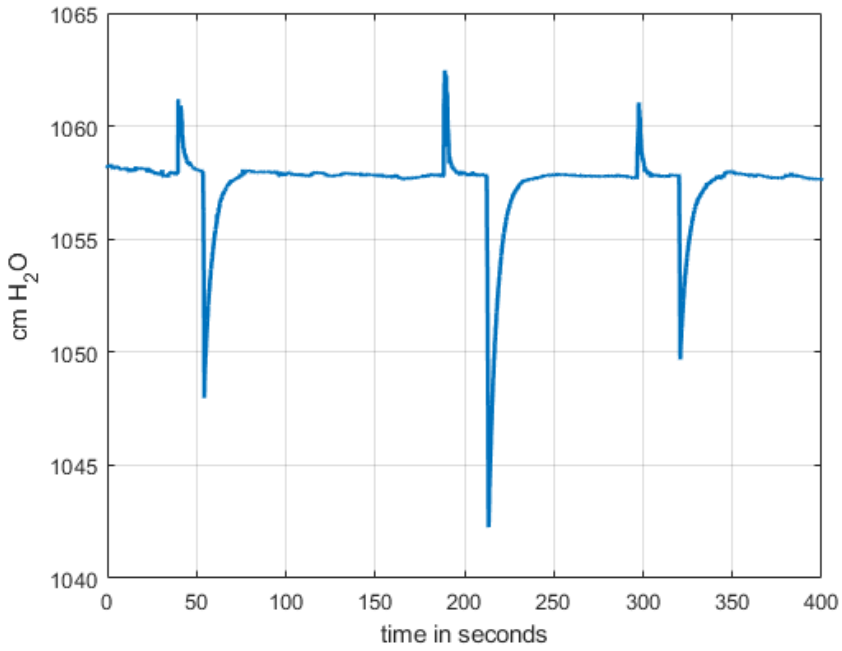

Figure A-4: All recovery curves from slug tests conducted at point E9 from 6/02/2017.

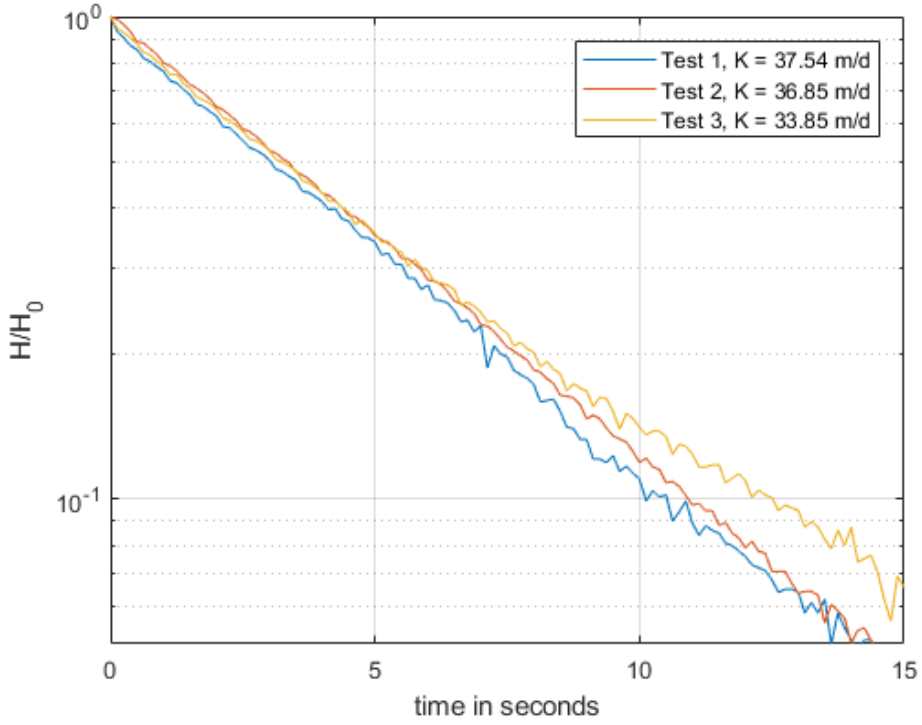

Figure A-5: Recovery curves from point E9 from 6/02/2017 where all measured heads (*H*) have been divided by the maximum observed head displacement (H_0), allowing for time lag comparison. Displayed *K* values are pre-temperature correction.

APPENDIX B: KRIGING ERROR AND STATISTICS

Method	Lag Size	Number of Lags	Number of Samples	Mean	Root Mean Square (RMS)	Mean Standard Deviation	RMS Standard Deviation	Average Standard Error
Stable	11.000	0.700	44.000	0.165	5.493	0.011	1.023	5.190
Gaussian	11.000	0.700	44.000	0.165	5.493	0.011	1.023	5.190
Exponential	11.000	0.700	44.000	0.052	5.610	0.026	0.911	6.055

Table B-1: Kriging statistics for *K* data from 6/02/2017, presented in figure 4-5.

Method	Lag Size	Number of Lags	Number of Samples	Mean	Root Mean Square (RMS)	Mean Standard Deviation	RMS Standard Deviation	Average Standard Error
Stable	13.000	0.700	44.000	0.001	4.915	0.013	1.015	4.940
Gaussian	13.000	0.700	44.000	0.004	5.117	0.026	1.177	4.523
Exponential	13.000	0.700	44.000	-0.004	4.837	0.005	0.923	5.279

Table B-2: Kriging statistics for *K* data from 7/05/2017, presented in figure 4-5.

Method	Lag Size	Number of Lags	Number of Samples	Mean	Root Mean Square (RMS)	Mean Standard Deviation	RMS Standard Deviation	Average Standard Error
Stable	10.000	0.700	44.000	0.087	5.853	-0.011	1.064	5.614
Gaussian	10.000	0.700	44.000	0.087	5.853	-0.011	1.064	5.614
Exponential	10.000	0.700	44.000	0.184	5.643	0.038	0.886	6.422

Table B-3: Kriging statistics for *K* data from 8/03/2017, presented in figure 4-5.

Method	Lag Size	Number of Lags	Number of Samples	Mean	Root Mean Square (RMS)	Mean Standard Deviation	RMS Standard Deviation	Average Standard Error
Stable	9	0.960	130.000	-0.074	5.429	-0.012	1.001	5.510
Gaussian	9	0.960	130.000	-0.074	5.429	-0.012	1.001	5.510
Exponential	9	0.960	130.000	-0.133	5.697	-0.020	0.720	7.947

Table B-4: Kriging statistics for K_v data from 6/02/2017, presented in figure 4-6.

Method	Lag Size	Number of Lags	Number of Samples	Mean	Root Mean Square (RMS)	Mean Standard Deviation	RMS Standard Deviation	Average Standard Error
Stable	7.000	1.330	130.000	-0.073	7.380	0.008	1.033	7.160
Gaussian	7.000	1.330	130.000	-0.073	7.380	0.008	1.033	7.160
Exponential	7.000	1.330	130.000	-0.111	7.358	-0.004	0.959	7.712

Table B-5: Kriging statistics for K_v data from 7/05/2017, presented in figure 4-6.

Method	Lag Size	Number of Lags	Number of Samples	Mean	Root Mean Square (RMS)	Mean Standard Deviation	RMS Standard Deviation	Average Standard Error
Stable	8.000	0.960	130.000	-0.089	6.690	-0.012	1.006	6.706
Gaussian	8.000	0.960	130.000	-0.089	6.690	-0.012	1.006	6.706
Exponential	8.000	0.960	130.000	-0.095	6.709	-0.013	1.002	6.726

Table B-6: Kriging statistics for K_v data from 8/03/2017, presented in figure 4-6.

Method	Lag Size	Number of Lags	Number of Samples	Mean	Root Mean Square (RMS)	Mean Standard Deviation	RMS Standard Deviation	Average Standard Error
Stable	3.750	12.000	1027.000	0.003	0.298	0.004	1.168	0.235
Gaussian	3.750	12.000	1027.000	0.004	0.377	0.011	0.594	0.517
Exponential	3.750	12.000	1027.000	0.004	0.304	-0.001	0.493	0.648

Table B-7: Kriging statistics for electromagnetic data from 6/15/2017, presented in figure 4-7.

Method	Lag Size	Number of Lags	Number of Samples	Mean	Root Mean Square (RMS)	Mean Standard Deviation	RMS Standard Deviation	Average Standard Error
Stable	5.000	7.000	1117.000	-0.001	0.284	-0.002	1.010	0.284
Gaussian	5.000	7.000	1117.000	0.000	0.305	0.005	0.626	0.485
Exponential	5.000	7.000	1117.000	0.003	0.325	0.004	0.565	0.655

Table B-8: Kriging statistics for electromagnetic data from 6/22/2017, presented in figure 4-7.

Method	Lag Size	Number of Lags	Number of Samples	Mean	Root Mean Square (RMS)	Mean Standard Deviation	RMS Standard Deviation	Average Standard Error
Stable	3.600	10.000	953.000	0.001	0.300	-0.009	1.394	0.282
Gaussian	3.600	10.000	953.000	-0.008	0.267	-0.011	0.674	0.391
Exponential	3.600	10.000	953.000	0.006	0.289	0.007	0.540	0.618

Table B-9: Kriging statistics for electromagnetic data from 6/29/2017, presented in figure 4-7.

Method	Lag Size	Number of Lags	Number of Samples	Mean	Root Mean Square (RMS)	Mean Standard Deviation	RMS Standard Deviation	Average Standard Error
Stable	3.800	12.000	1014.000	-0.006	0.719	-0.003	0.936	0.760
Gaussian	3.800	12.000	1014.000	-0.006	0.719	-0.003	0.936	0.760
Exponential	3.800	12.000	1014.000	0.020	0.623	0.018	0.685	0.969

Table B-10: Kriging statistics for electromagnetic data from 8/09/2017, presented in figure 4-7.